ARTICLE

Mesozoic porphyry Cu–Au mineralization and associated adakite-like magmatism in the Philippines: insights from the giant Atlas deposit

Yu Zhang [1,2] · Jing Tian [1,3] · Pete Hollings [4] · Lin Gong [1,3] · Iglas Alburo [5] · Al Emil Berador [6] · Dennis G. Francisco [5] · Jie Li [7] · Huayong Chen [1,3]

Abstract

The Atlas porphyry Cu–Au deposit is located in central Cebu Island in the Philippines, with a proven mineral reserve of 1420 Mt at 0.45% Cu, 0.24 g/t Au, 0.018 g/t Mo, and 1.8 g/t Ag. It is associated with the Lutopan quartz diorite porphyry stock that was emplaced into the Cretaceous volcano-sedimentary sequences of the Cansi Formation. Two stages of hypogene alteration have been identified at Atlas: stage I quartz–magnetite ± chalcopyrite ± pyrite veins associated with potassic and propylitic alteration and stage II anhydrite–pyrite–chalcopyrite ± specularite veins associated with phyllic alteration. Supergene gypsum veins are also present. Mineralization is mainly associated with the stage I and stage II veins. The Lutopan quartz diorite porphyry yielded a zircon U–Pb age of 108.5 ± 1.6 Ma and is characterized by high Sr/Y (54–69), with the corresponding magma having high oxygen fugacity (avg. ΔFMQ +2.7, avg. Ce^{4+}/Ce^{3+} of zircon = 439) and H_2O concentrations (presence of amphibole and biotite phenocrysts) and low magmatic temperatures (avg. Ti-in-zircon thermometry = 706 °C). The relatively low La/Yb ratios (9–11), listric-shaped normalized REE patterns with weak or absent Eu anomalies, together with zircon $\varepsilon_{Hf}(t)$ values of 3.4 to 10.0, whole-rock I_{Sr} values of 0.70373–0.70382, $\varepsilon_{Nd}(t)$ values of 2.4–3.4 and Mg numbers of 49–53 suggest that the Lutopan quartz diorite porphyry was likely derived from partial melting of young lower continental crust or interaction between asthenospheric melts and lower crust melts, that evolved to adakite-like trace element compositions through amphibole fractionation. Stage I veins yielded a pyrite Re–Os isochron age of 110.2 ± 5.6 Ma, making Atlas the only Mesozoic porphyry deposit discovered in the Philippines.

Keywords Atlas porphyry Cu–Au deposit · Mesozoic · Zircon geochemistry and isotope · Pyrite Re–Os geochronology · Philippines

✉ Huayong Chen
huayongchen@gig.ac.cn

1 Key Laboratory of Mineralogy and Metallogeny, Guangzhou Institute of Geochemistry, Chinese Academy of Sciences, Guangzhou 510640, China

2 School of Geosciences and Info-Physics, Central South University, Changsha 410083, China

3 University of Chinese Academy of Sciences, Beijing 100049, China

4 Department of Geology, Lakehead University, 955 Oliver Road, Thunder Bay, Ontario P7B 5E1, Canada

5 Carmen Copper Corporation, 6038 Toledo, Philippines

6 Regional Office 7, Mines & Geosciences Bureau, Philippine Department of Environment & Natural Resources, 6014 Mandaue, Philippines

7 Key Laboratory of Isotope Geochronology and Geochemistry, Guangzhou Institute of Geochemistry, Chinese Academy of Sciences, Guangzhou 510640, China

Introduction

Porphyry deposits typically occur in narrow, linear metallogenic provinces, that mostly formed in modern or ancient convergent margin settings (Kesler 1997; Sillitoe 2010; Chiaradia et al. 2012; Richards 2013a, b), and notably around the Pacific (Sillitoe 2000; Cooke et al. 2005).

The Philippine archipelago is located at the boundary of the Eurasian and West Philippine Sea plates (Castillo et al. 1999; Yumul et al. 2000). These converging plates constrain the Philippine Mobile Belt, an actively deforming tectonic collage of oceanic crustal blocks bounded to the east and west by subduction zones (Fig. 1; Rangin et al. 1999; Aurelio 2000; Yumul 2003; Ozawa et al. 2004). Previous studies have shown that porphyry mineralization in magmatic arcs has occurred in the Philippine archipelago since the Cretaceous (Walther et al. 1981; Yumul et al. 2008; Hollings et al. 2011a, b; Aurelio et al. 2013). Many porphyry deposits crop out along the Philippine Mobile Belt, with the majority in the Negros–Marinduque area (30–15 Ma), eastern Luzon (23–11 Ma), north–central Luzon (10.5–0.99 Ma), NE Mindanao (11.2–1.6 Ma), and SE Mindanao (5.4–3.3 Ma; Divis 1983; Sillitoe and Gappe 1984; Yumul et al. 2003; Hammarstrom et al. 2010; Hollings et al. 2011a). A small number of porphyry deposits has been reported in the Cebu–Bohol area with possible Mesozoic ages (110–95 Ma; Walther et al. 1981; Divis 1983). The Cenozoic porphyry deposits have been the focus of considerable research (e.g., Wolfe et al. 1978; Hedenquist et al. 1998; Arribas et al. 1995; Tarkian and Koopmann 1995; Shinohara and Hedenquist 1997; Braxton et al. 2009, 2012, 2018; Braxton and Mathur 2011; Cooke et al. 2011; Wolfe and Cooke 2011; Hollings et al. 2013; Cao et al. 2018), whereas the Philippine Mesozoic porphyry deposits lack the same level of detailed study.

The giant Atlas porphyry Cu–Au deposit (1420 Mt at 0.45% Cu, 0.24 g/t Au, 0.018 g/t Mo, 1.8 g/t Ag; Singer et al. 2008), located in central Cebu Island, has been argued to be the oldest Philippine porphyry deposit based on whole-rock Rb–Sr (107.6 ± 2.9 Ma) and K–Ar (95 ± 5 Ma) ages of the mineralized intrusion (Walther et al. 1981). We report U–Pb dating results of zircon from the mineralized intrusion to constrain the mineralization age at Atlas. This study also reports the results of new field observations, whole-rock and zircon geochemistry of the mineralized intrusion, as well as pyrite Re–Os dating to investigate (1) the nature and geochemical characteristics of the mineralized intrusion at Atlas, (2) the age of mineralization, and (3) the Mesozoic metallogenic history of the Philippines.

Geological setting

Regional geology

The Philippine archipelago is made up of the aseismic Palawan Microcontinental Block and the seismically-active Philippine Mobile Belt which is characterized by earthquakes and active volcanoes (Balce 1980; Yumul 2007; Yumul et al. 2008; Walia et al. 2012). Pre-Jurassic quartz-rich sandstones, slates, phyllites, and schists in the Palawan Microcontinental Block, including the northern Palawan, Mindoro, and the Zamboanga peninsula of Mindanao (Fernandez 1981), suggest a continental affinity for the basement of the southwestern Philippines (Fig. 1). In contrast, greenschist-facies metavolcanic rocks, and ophiolitic mafic to ultramafic basement rocks (including serpentinites, gabbros, and amphibolites) in the Philippine Mobile Belt have an oceanic crustal affinity (Faure et al. 1989; Yumul et al. 1997; Aurelio 2000; Polve et al. 2007).

The Central Philippines (Visayas) is made up of the islands of Panay, Negros, Cebu, Bohol, Leyte, and Samar. The Cretaceous-Eocene basement rocks in Visayas are defined by intact to dismembered crust–mantle sequences with regionally metamorphosed rocks, intrusive rocks and volcano-sedimentary sequences (Fig. 1; Deng et al. 2015).

Cebu Island consists of a basement complex of lherzolites and harzburgites, Jurassic metamorphic and Cretaceous volcanic rocks, and Cretaceous sedimentary units (Dimalanta et al. 2006). These rocks are exposed mostly in the central portion of the island (Deng et al. 2015). The oldest Jurassic Tunlob Formation in the district is composed of chloritic orthoschist and micaceous paraschist that has been metamorphosed to albite–epidote–amphibolite facies (Aurelio and Peña 2002). These rocks are unconformably overlain by the Cretaceous Managa Group, which consists of the basal Early Cretaceous Cansi Formation and the overlying Late Cretaceous Pandan Formation (Aurelio and Peña 2002). The Cansi Formation is mainly composed of basaltic and andesitic volcaniclastic sandstone, with limestone intercalations, whereas the Pandan Formation consists of conglomerate, sandstone and shale, with basalt, limestone, and coal intercalations (Philippine Bureau of Mines and Geosciences 1986; Aurelio and Peña 2002; Deng et al. 2015). A series of northeast-trending faults in the central district of Cebu have influenced the emplacement of igneous rocks, serving as conduits for magmatism. Pre-Pliocene quartz diorite intrusions and andesitic rocks occur in a northwest-trending belt extending from southeastern Bohol to the central highlands of Cebu (Hammarstrom et al. 2010). These intrusions are primarily NE-trending (quartz) diorite stocks (Hammarstrom et al. 2010).

Deposit geology

The Atlas Cu–Au deposit is situated approximately 30 km west of Cebu City on Cebu Island, Philippines (Fig. 1). The volcano-sedimentary strata that crop out in the mining area primarily consist of the Cretaceous Managa Group (Cansi and Pandan formations) and the Oligocene Naga Formation (Philippine Bureau of Mines and Geosciences 1986; Fig. 2). The Pandan Formation comprises metamorphosed pillowed mafic volcanic
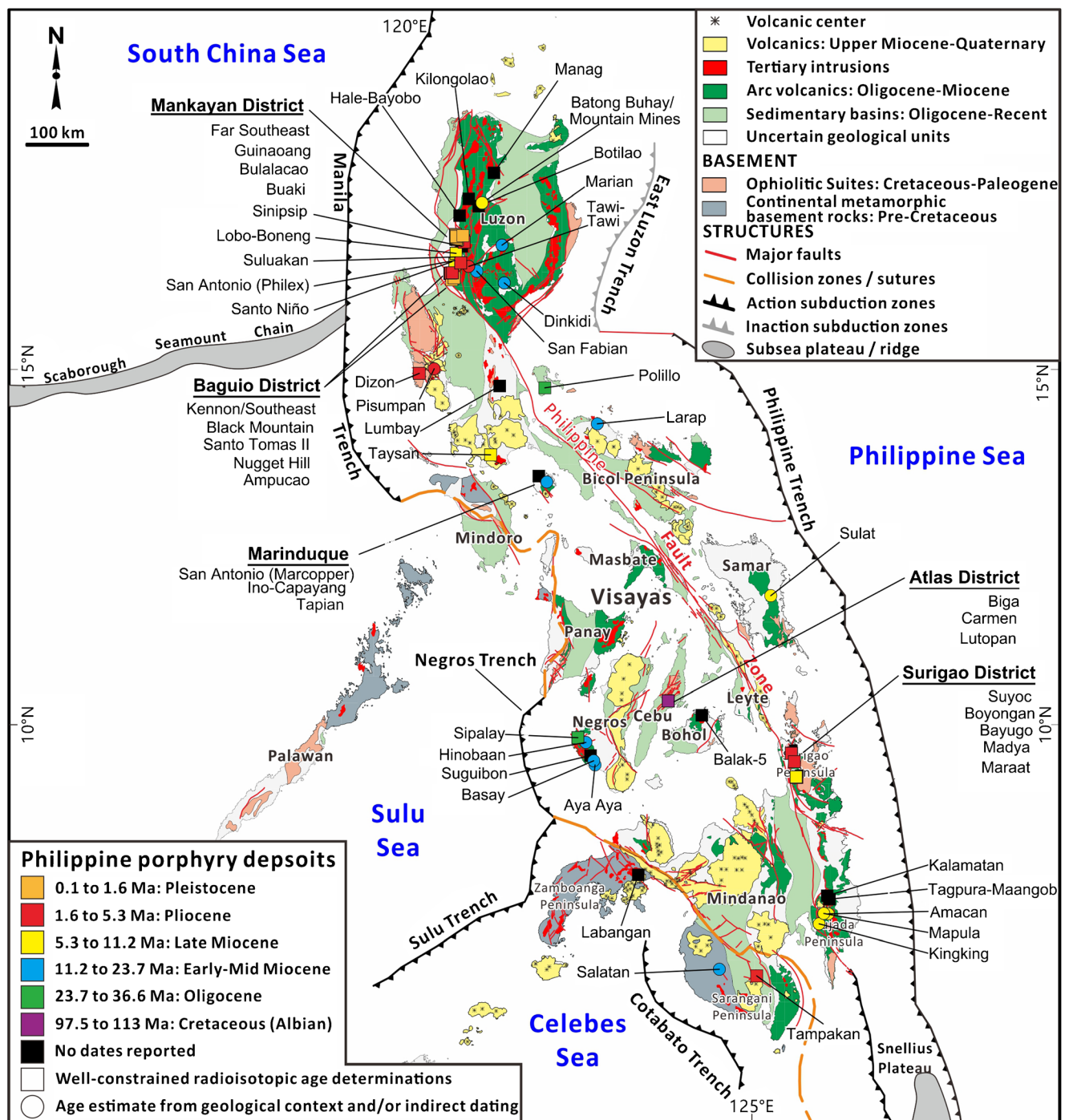
Fig. 1 Regional geology of the Philippine archipelago and distribution of porphyry deposits throughout the Philippine archipelago (after Braxton 2007; Braxton et al. 2018)

rocks with intercalated lithic tuff and wackes whereas the Cansi Formation is predominantly comprised of andesitic volcanic rocks (Sillitoe and Gappe 1984; Philippine Bureau of Mines and Geosciences 1986). The Oligocene Naga Formation is composed of mudstone and shale, with some limestone intercalations. The ENE-trending North Barot and Cantabaco right-lateral strike-slip faults, considered to have been at least partially responsible for detachment, transport, and juxtaposition of

allochthonous terranes in the Philippines (Sillitoe and Gappe 1984), define a ~ 3.5 km wide horst and are interpreted to have played a major role in the localization of the ore bodies (Fig. 2; Madamba 1972; Divis 1983; Philippine Bureau of Mines and Geosciences 1986; Hammarstrom et al. 2010). Uplift of the horst resulted in the erosion of the sedimentary cover, the development of the present geomorphology, and facilitated the discovery of the Atlas deposit (Madamba 1972; Divis 1983). The Sudlon
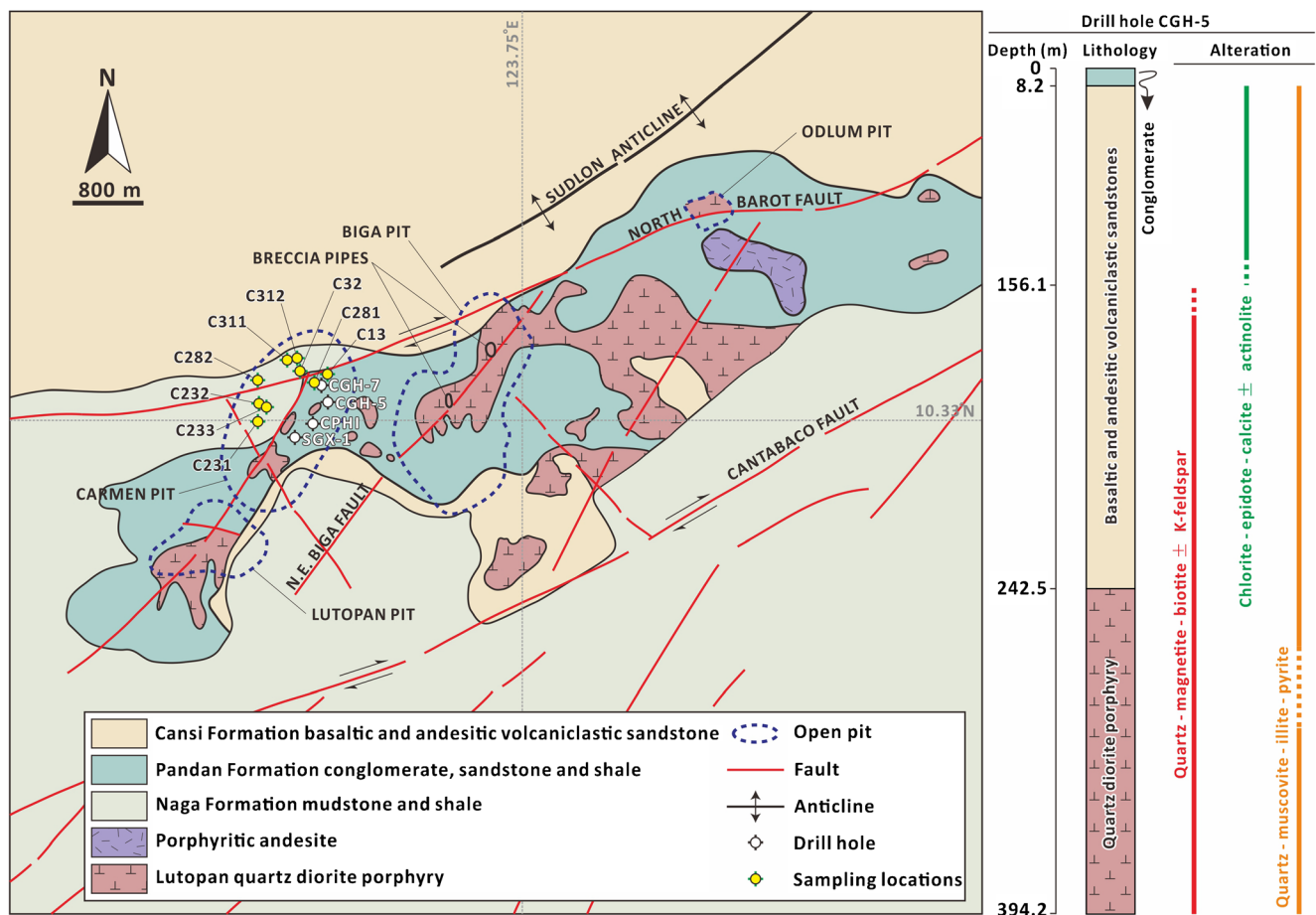
Fig. 2 Geological map of the Atlas Cu–Au deposit (modified after Divis 1983) and columnar section of drill hole CGH-5

anticline occurs in the north of the mining area with an axis parallel to the North Barot and Cantabaco faults. At Biga, two breccia pipes occur along the NE-oriented Biga Fault (Fig. 2). They are tabular with strike lengths of 150 m and extend to depths of more than 3000 m. The breccia is composed of angular fragments (1–3 cm) of quartz diorite porphyry and rare volcaniclastic sandstone (Philippine Bureau of Mines and Geosciences 1986). The dominant igneous rock at Atlas is the Lutopan stock which crops out between the North Barot and Cantabaco faults and intruded the Cretaceous Cansi Formation, with minor porphyritic andesite in the northeastern of the district (Divis 1983; Deng et al. 2015). The Lutopan stock has a northeast-trending elongated shape (Fig. 2), with length/width ratios of ca. 14 and 8 at Carmen and Lutopan, respectively (Sillitoe and Gappe 1984), and approaches an irregular mushroom shape with a "stem" width of ca. 150 m extending more than 450 m vertically (Madamba 1972; Philippine Bureau of Mines and Geosciences 1986). The stock is primarily a quartz diorite porphyry (Fig. 2). It is medium- to coarse-grained, gray in color and massive with a porphyritic texture (Fig. 3a). The rocks contain ~75 vol% phenocrysts (~50 vol%

plagioclase, ~25 vol% amphibole and minor biotite) in a microcrystalline quartz and feldspar groundmass (Fig. 3b). Minor magnetite, zircon, and apatite occur as accessory minerals. Plagioclase is typically 0.5–1.0 mm in size and has euhedral to subhedral slab textures (Fig. 3b) with Carlsbad twinning (Fig. 3c), and locally is well zoned. Amphibole is 1.0–1.5 mm in size and occurs as simple twins. Additionally, the quartz diorite porphyry shows multiphase features including local fine-grained diorite inclusions (Fig. 3d).

Alteration and mineralization

The three major orebodies at Atlas are Lutopan, Biga, and Carmen. They are located in the southwestern, western, and central portions of the district (Fig. 2). The orebodies are lenticular, elongated, and are localized along the intersection of the NE trending faults (e.g., Biga Fault) with the main North Barot and Cantabaco right-lateral strike-slip faults (Fig. 2; Sillitoe and Gappe 1984) and are mostly confined to the Lutopan stock (Divis 1983). The Atlas orebodies all dip east to southeast at 40–65°, which has been attributed to the post-mineralization
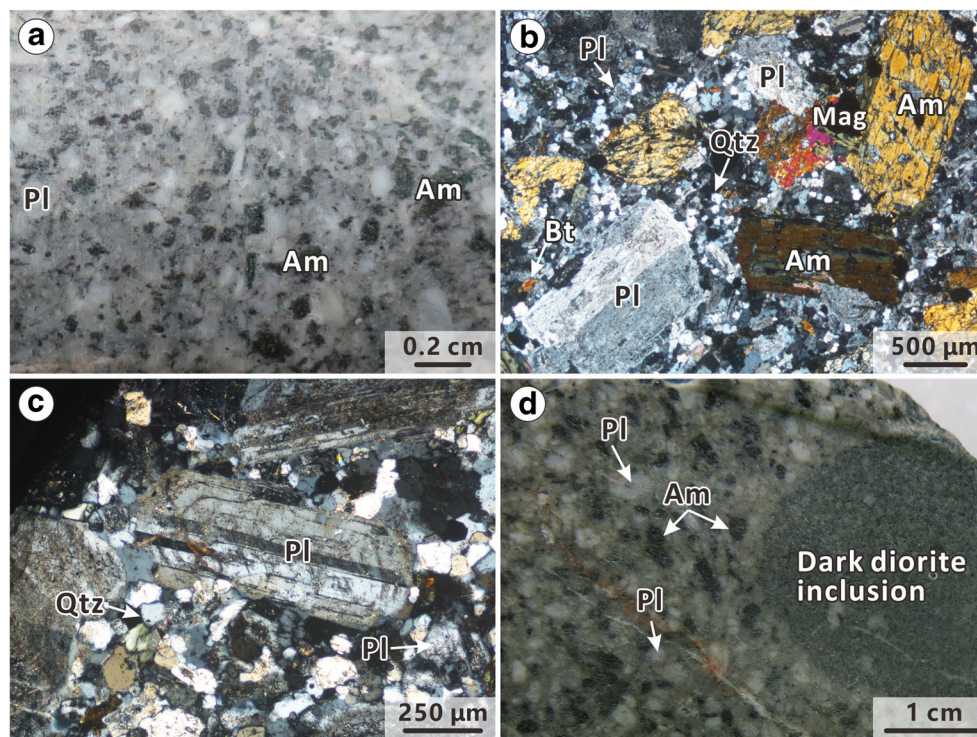
Fig. 3 Photographs showing representative mineral assemblages, textural features, and diorite inclusions of the Lutopan quartz diorite porphyry. **a** The Lutopan quartz diorite porphyry contains plagioclase and amphibole phenocrysts generally < 0.2 cm (10° 20′ 0.25″ N, 123° 43′ 46.58″ E, elevation = 91 m). **b** Plagioclase and amphibole phenocrysts of the Lutopan quartz diorite porphyry in a fine-grained groundmass of plagioclase, quartz, and biotite. The majority of fine-grained biotite is secondary (CPL; 10° 20′ 0.25″ N, 123° 43′ 46.58″ E, elevation = 112 m). **c** Carlsbad-twinning plagioclase phenocryst in a fine-grained groundmass of plagioclase and quartz (CPL; same sample as **b**). **d** Dark fine-grained diorite inclusion in the Lutopan quartz diorite porphyry, showing the multiphase feature of the Lutopan stock (10° 20′ 19.40″ N, 123° 43′ 53.30″ E, elevation = −296 m). Pl plagioclase, Am amphibole, Mag magnetite, Qtz quartz, Bt biotite

westward tilting of the block bounded by the North Barot and Cantabaco faults (Sillitoe and Gappe 1984). The Lutopan orebody is located mainly in the stem of the Lutopan quartz diorite porphyry and extends about 120 m into the footwall volcanic rocks and 60 m into the hanging wall. At the Lutopan orebody, up to 10 vol% sulfides with a pyrite/chalcopyrite ratio of about 5 has been reported in the hanging wall, decreasing to 1.5 vol% with a pyrite/chalcopyrite ratio of about 0.5 in the footwall (Philippine Bureau of Mines and Geosciences 1986). The mineralized zones at Biga and Carmen extend up to about 1500 m in length and 450 m in width and have a north-northeast strike (Madamba 1972). The Biga orebody occurs around two breccia pipes (Fig. 2), but the pipes themselves are only weakly mineralized with a small amount of quartz–pyrite–chalcopyrite in the matrix (Philippine Bureau of Mines and Geosciences 1986). The small Odlum orebody occurs in the northeast of the Atlas mining area (Fig. 2) and has been proposed to be the result of post-mineralization right-lateral translation of the northern tip of the Biga orebody along the North Barot Fault (Sillitoe and Gappe 1984).
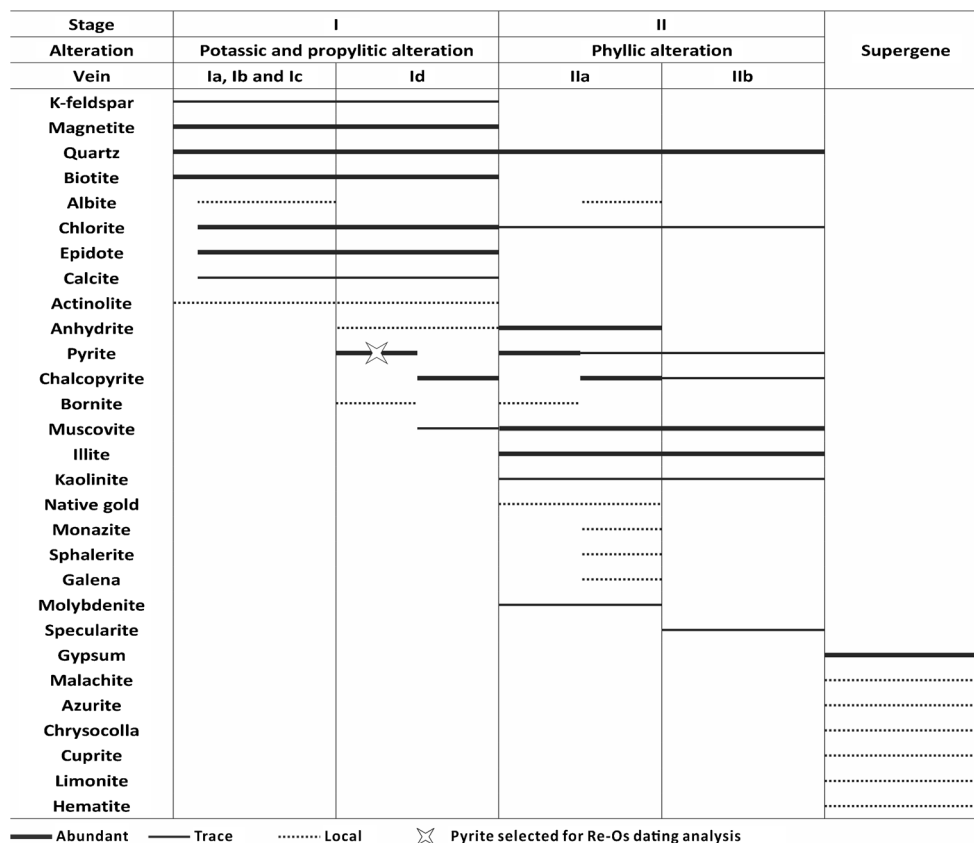
Based on crosscutting and overprinting relationships combined with petrographic analysis, including systematic short wavelength infrared (SWIR) spectral analyses (TerraSpec, Analytical Spectral Devices, Inc.: ASD), six types of veining

and related hypogene alteration associated with the Lutopan stock have been identified. These veins and alteration stages are classified into two groups: stage I and stage II. In addition late supergene gypsum veins have overprinted the hypogene features (Fig. 4; Philippine Bureau of Mines and Geosciences 1986). Alteration and vein stages are described below from oldest to youngest.

Stage I potassic and propylitic alteration

Stage I potassic alteration (quartz–magnetite–biotite ± K-feldspar) is concentrically distributed around the Lutopan stock and characterized by abundant secondary hydrothermal biotite (~ 10 vol%) and local K-feldspar (< 5 vol%) coexisting with abundant quartz and magnetite, and trace actinolite (Sillitoe and Gappe 1984). This stage affected the majority of the Lutopan stock and some basaltic and andesitic volcaniclastic sandstones. Ferromagnesian minerals (most likely amphibole) in the quartz diorite porphyry have been altered to fine-grained secondary biotite with magnetite and quartz, which occur throughout the groundmass, whereas plagioclase phenocrysts are generally unaltered (Fig. 5a). Locally within the core of the alteration zone, biotite occurs as clots with quartz and magnetite, which may have nucleated on the margins of

Fig. 4 Alteration and mineral paragenesis of the Atlas deposit. See text for detailed description of alteration and mineralization

Stage	I		II		Supergene
Alteration	**Potassic and propylitic alteration**		**Phyllic alteration**		**Supergene**
Vein	**Ia, Ib and Ic**	**Id**	**IIa**	**IIb**	
K-feldspar	▬▬▬				
Magnetite	▬▬▬	▬▬			
Quartz	▬▬▬	▬▬	▬▬		
Biotite	▬▬▬				
Albite	··········		··········		
Chlorite	▬▬▬	▬▬			
Epidote	▬▬▬	▬▬			
Calcite	▬▬				
Actinolite	··········	······			
Anhydrite		·········	▬▬		
Pyrite		☆▬▬	▬▬	▬▬	
Chalcopyrite		▬▬	▬▬	▬▬	
Bornite		······	······		
Muscovite			▬▬	▬▬	
Illite			▬▬	▬▬	
Kaolinite			▬▬	▬▬	
Native gold			··········		
Monazite			··········		
Sphalerite			··········		
Galena			··········		
Molybdenite			▬▬		
Specularite				▬▬	
Gypsum					▬▬▬
Malachite					··········
Azurite					··········
Chrysocolla					··········
Cuprite					··········
Limonite					··········
Hematite					··········

▬▬ **Abundant**   ▬ **Trace**   ········· **Local**   ☆ **Pyrite selected for Re-Os dating analysis**

primary amphibole phenocrysts. Potassium feldspar occurs as pervasive alteration and has largely obliterated primary textures in the igneous rocks.

Stage I propylitic alteration (chlorite–epidote ± calcite ± actinolite) contains abundant chlorite and epidote, with minor calcite and actinolite, and passes laterally inward to the potassic alteration zone. The propylitic alteration zone shows no distinct boundary with the potassic zone and extends at least 1 km away from the potassic zone, but the outer limit is poorly defined due to limited drilling. In the propylitic zone, the fine-grained ferromagnesian minerals (amphibole and biotite) in the basaltic and andesitic volcaniclastic sandstones of the Cansi Formation commonly have been altered to fine-grained chlorite and epidote with minor calcite and actinolite. Locally, chlorite and epidote selectively replaced secondary hydrothermal biotite that occurred with magnetite, indicating that the propylitic alteration locally overprinted the potassic alteration.

Stage I veins

Stage I veins are characterized by the presence of magnetite associated with potassic alteration. Only a small number of barren quartz–chlorite and epidote veins have been observed associated with the propylitic alteration. Four main types of stage I veins occur: (1) straight-sided magnetite veins (stage

Ia, dominant magnetite with less than 10% quartz; Fig. 5b), (2) straight-sided quartz–biotite–magnetite veins (stage Ib; Fig. 5c), (3) wavy or straight-sided quartz–magnetite veins (stage

Fig. 5 Photographs showing representative mineral assemblages and textural features of alteration and associated veins at Atlas. **a** Amphibole phenocrysts have been selectively altered to fine-grained secondary biotite intergrown with fine-grained quartz and magnetite occurring in the groundmass, compared to stable plagioclase phenocrysts (CPL; 10° 20′ 10.02″ N, 123° 43′ 49.95″ E, elevation = 110 m). **b** Stage Ia vein with discontinuous and irregular alteration envelops of K-feldspar intergrown with albite cut by later supergene gypsum vein (10° 20′ 7.6″ N, 123° 43′ 51.46″ E, elevation = 21 m). **c** Typical expression of the wavy stage Ic vein cutting the straight-sided stage Ib vein in the intense potassic alteration zone (PPL; same sample as **a**). **d** Stage Id vein with pyrite–chalcopyrite central band, truncating stage Ic vein (10° 20′ 11.38″ N, 123° 43′ 48.46″ E, elevation = −151 m). **e** Chalcopyrite intergrown with minor quartz, muscovite, and magnetite has replaced pyrite grains in stage Id vein (10° 20′ 5.30″ N, 123° 43′ 30.57″ E, elevation = 249 m). **f** Muscovite and illite replaced original plagioclase and secondary biotite from potassic alteration, showing that stage II phyllic alteration overprinted stage I potassic alteration (CPL; 10° 20′ 12.22″ N, 123° 43′ 48.59″ E, elevation = 109 m). **g** Stage IIa vein with alteration envelope of quartz–muscovite–illite–pyrite cutting stage Id vein (10° 20′ 19.93″ N, 123° 43′ 42.66″ E, elevation = 233 m). **h** Chalcopyrite network vein, coexisting with sphalerite, galena, and native gold crosscut the earlier pyrite grains in the stage IIa vein (10° 20′ 5.24″ N, 123° 43′ 33.01″ E, elevation = 243 m). Ab albite, Bt biotite, Ccp chalcopyrite, Gn galena, Gp gpysum, Ill illite, Kfs K-feldspar, Mag magnetite, Ms muscovite, Ng native gold, Pl plagioclase, Py pyrite, Qtz quartz, Sp sphalerite
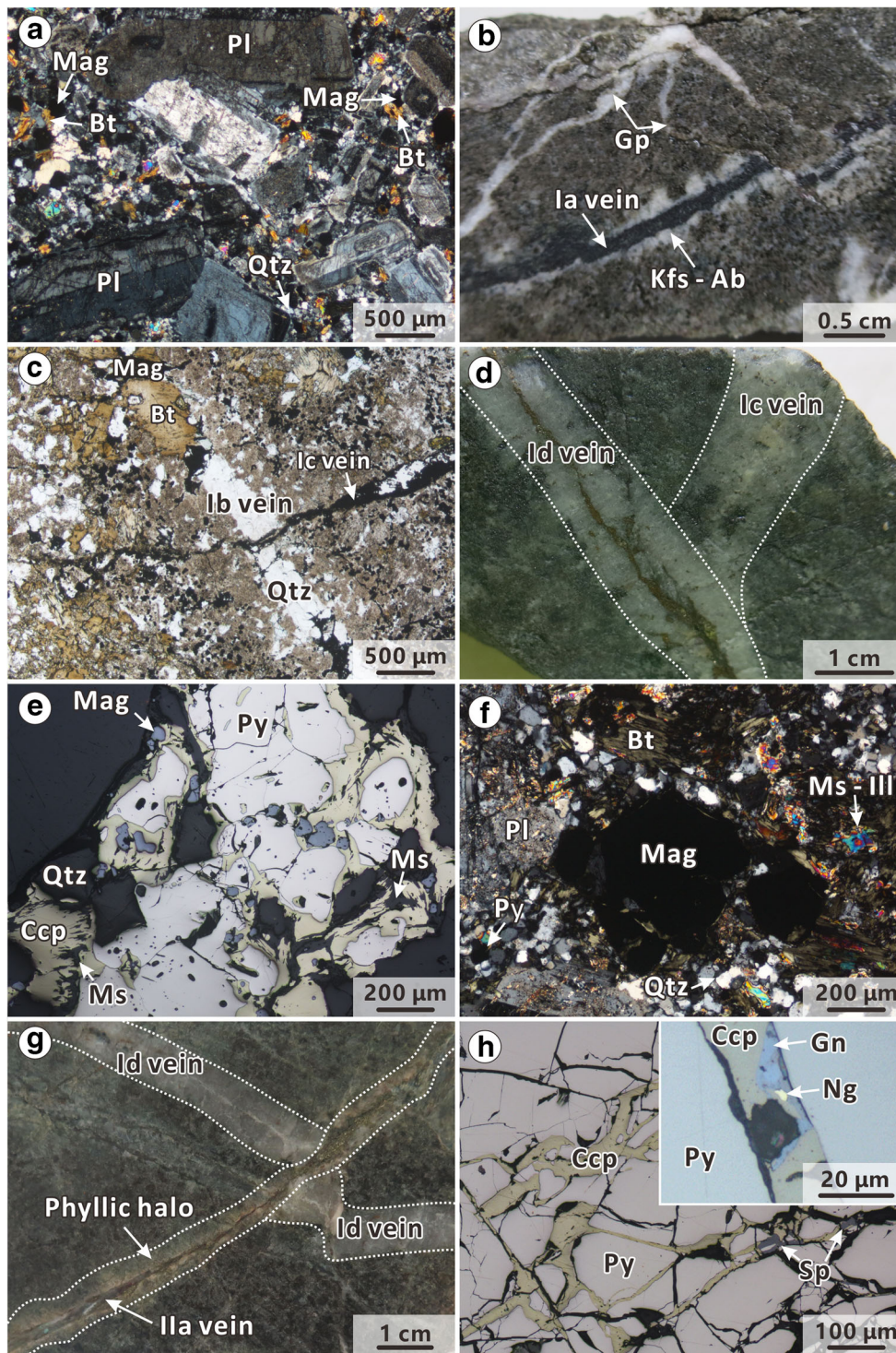
Ic; Fig. 5c and d), and (4) straight-sided quartz–magnetite–pyrite–chalcopyrite veins (stage Id; Fig. 5d).

Stage Ia veins are primarily composed of magnetite and only developed in the core of the potassic zone at Atlas. This vein stage generally ranges from 0.2 to 0.5 cm in width with irregular, discontinuous alteration halos (commonly 0.2 to 0.3 cm in width) of pale K-feldspar intergrown with albite (Fig. 5b).

Stage Ib veins (commonly ca. 0.2 to 1.0 cm in width) are characterized by anhedral biotite intergrown with magnetite in veined quartz (Fig. 5c) and are most intensely developed within and adjacent to the Lutopan quartz diorite porphyry. Stage Ib veins locally truncate stage Ia veins and lack alteration envelopes.

Stage Ic veins (ca. 0.2 to 1.0 cm wide) are hosted within and adjacent to the Lutopan quartz diorite porphyry and lack alteration envelopes like stage Ib veins, but are distinct from

stage Ib veins in that they lack biotite (Fig. 5 c and d). In these veins, quartz commonly shows variable internal structures as continuous vein-wall coatings or small discontinuous lines in the straight-sided veins, or irregular grains in the wavy veins. In most cases, stage Ic veins truncate stage Ib veins (Fig. 5c), although the reverse has been observed in a few samples, indicating that these two vein stages were broadly coeval.

Stage Id veins (commonly ~ 0.8–2.0 cm in width) are the final vein stage associated with potassic alteration and represent one of the major mineralization types at Atlas. This vein stage is characterized by the presence of abundant pyrite and chalcopyrite with minor amounts of magnetite (Fig. 5d). Stage Id veins locally truncate stage Ic veins and lack alteration envelopes (Fig. 5d). In stage Id veins, pyrite occurs as anhedral crystals and coexists with quartz and minor bornite. However, abundant chalcopyrite commonly formed later than pyrite, consistent with chalcopyrite intergrown with quartz, muscovite, and magnetite replacing pyrite (Fig. 5e) or formed along the boundary of pyrite grains.

Stage II phyllic alteration

Stage II phyllic alteration (quartz–muscovite–illite ± pyrite) is characterized by abundant quartz, muscovite, and illite (identified by SWIR analysis), with minor disseminated pyrite. It overprinted parts of the earlier potassic and propylitic alteration zones (Fig. 2). Muscovite and illite have commonly replaced primary plagioclase in the Lutopan quartz diorite porphyry and secondary biotite in potassic altered rocks (Fig. 5f). Locally, phyllic alteration is pervasive, obliterating the earlier potassic alteration features and primary textures of the Lutopan stock. Sillitoe and Gappe (1984) reported that the illite–kaolinite–chlorite alteration constitutes a subsidiary mineral assemblage of phyllic alteration at Atlas, and this alteration is characterized by illite–kaolinite alteration of plagioclase phenocrysts and chlorite replacement of amphibole phenocrysts in the quartz diorite porphyry.

Stage II veins

Stage II veins are characterized by abundant pyrite and chalcopyrite associated with phyllic alteration which occurs as halos around anhydrite–specularite–pyrite–chalcopyrite veins. Two generations of stage II veins have been identified, namely (1) anhydrite–pyrite–chalcopyrite veins (stage IIa veins; Fig. 5g) and (2) specularite–pyrite–chalcopyrite veins (stage IIb veins).

Stage IIa veins (primarily 1–3 cm wide, locally up to ~ 15 cm wide) are composed of abundant anhydrite, pyrite, and chalcopyrite with minor amounts of sphalerite, galena, and native gold. Pyrite and chalcopyrite commonly occur as bands in the vein. Locally, small amounts of molybdenite occur as coatings along stage

IIa veins. Where observed, stage IIa veins cut stage Id veins and have alteration envelopes of quartz–muscovite–illite–pyrite in the phyllic alteration zone (Fig. 5g). In stage IIa veins, pyrite coexists with trace bornite and native gold, often showing exsolution textures, but they are distinct from stage Id pyrite because of the absence of quartz and the occurrence of anhydrite and native gold. Chalcopyrite in the veins crosscuts the pyrite (Fig. 5h). The chalcopyrite commonly coexists with sphalerite, galena, native gold (Fig. 5h), monazite, and albite in stage IIa veins, distinct from the muscovite, magnetite, and quartz assemblage in stage Id veins (Fig. 5e).

Stage IIb veins (~ 0.1 to 0.8 cm in width) are characterized by specularite and represent the final mineralization event. The morphology of this vein stage is variable, commonly occurring with obvious alteration halos of quartz–muscovite–illite or as irregular lines. Specularite commonly occurs as irregular lines or grains, coexisting with minor pyrite and chalcopyrite. Stage IIb veins crosscut stage IIa veins.

## Supergene gypsum veins and Cu-Fe minerals

Abundant barren gypsum veins (ca. 0.2–1.0 cm) are uniformly distributed throughout both orebodies and host rocks, and crosscut stage I and II veins (Fig. 5b). This gypsum has been proposed to be the product of supergene hydration by cold meteoric waters (Sillitoe and Gappe 1984). On the surface of the Atlas deposit, some secondary copper minerals (malachite, azurite, chrysocolla, and cuprite) occur as paints or stains, whereas secondary iron minerals (limonite and hematite) occur as coatings along fractures (Philippine Bureau of Mines and Geosciences 1986). All of them were formed during weathering of the Atlas deposit.

Sampling and analytical techniques

Three quartz diorite porphyry samples (CPHI-1, CPHI-3, and SGX-1) from the Lutopan stock were collected for petrographic and geochemical study. The samples are distal to the mineralized section, minimizing the influence of hydrothermal alteration on whole-rock geochemistry. Their locations are listed in ESM 1. Twenty zircon grains were separated from CPHI-3 for U–Pb–Hf analysis.

Nine pyrite samples were collected from the Carmen orebody for Re–Os dating. Four samples (C281, C282, C231, and C232) were from stage Id veins, whereas the others (C233, C13, C311, C312, and C32) were from stage IIa veins. Their locations are shown in Fig. 2 and listed in ESM 2. Samples C281, C282, C231, and C232 are stage Id veins with widths of ~ 1–2 cm, and pyrite and chalcopyrite commonly occur as bands and irregular dissemination in the vein (e.g., C232, Fig. 6a). In the veins, pyrite occurs as anhedral grains and shows no obvious multi-stage

Fig. 6 Photographs showing representative textural features of pyrite for Re–Os analysis from stage Id veins and stage IIa veins. **a** Pyrite and chalcopyrite occurring as bands and irregular dissemination in the stage Id vein (C232). **b** Anhedral pyrite grain in stage Id veins (C281). **c** Pyrite and chalcopyrite occurring as irregular masses in the stage IIa vein (C32). **d** Cataclastic pyrite grains with abundant irregular fine fractures (C233). **e** Reflected-light microphotograph of stage Id pyrite grain from C281, fully etched with NaOCl exhibiting homogeneous brown color and no internal texture. **f** Stage Ia pyrite grain from C282 fully etched with NaOCl exhibiting homogeneous purple color and no internal texture under reflected light. **g** Reflected-light microphotograph of pyrite grain (C312 of stage IIa vein) fully etched with NaOCl exhibiting irregular zoned texture. **f** Pyrite grain in C32 (stage IIa vein) showing irregular zoned texture and pyrite inclusion by etching with NaOCl. The locations of samples for Re–Os analysis are listed ESM 2. Adr anhydrite, Bn bornite. Other abbreviations as in Fig. 5
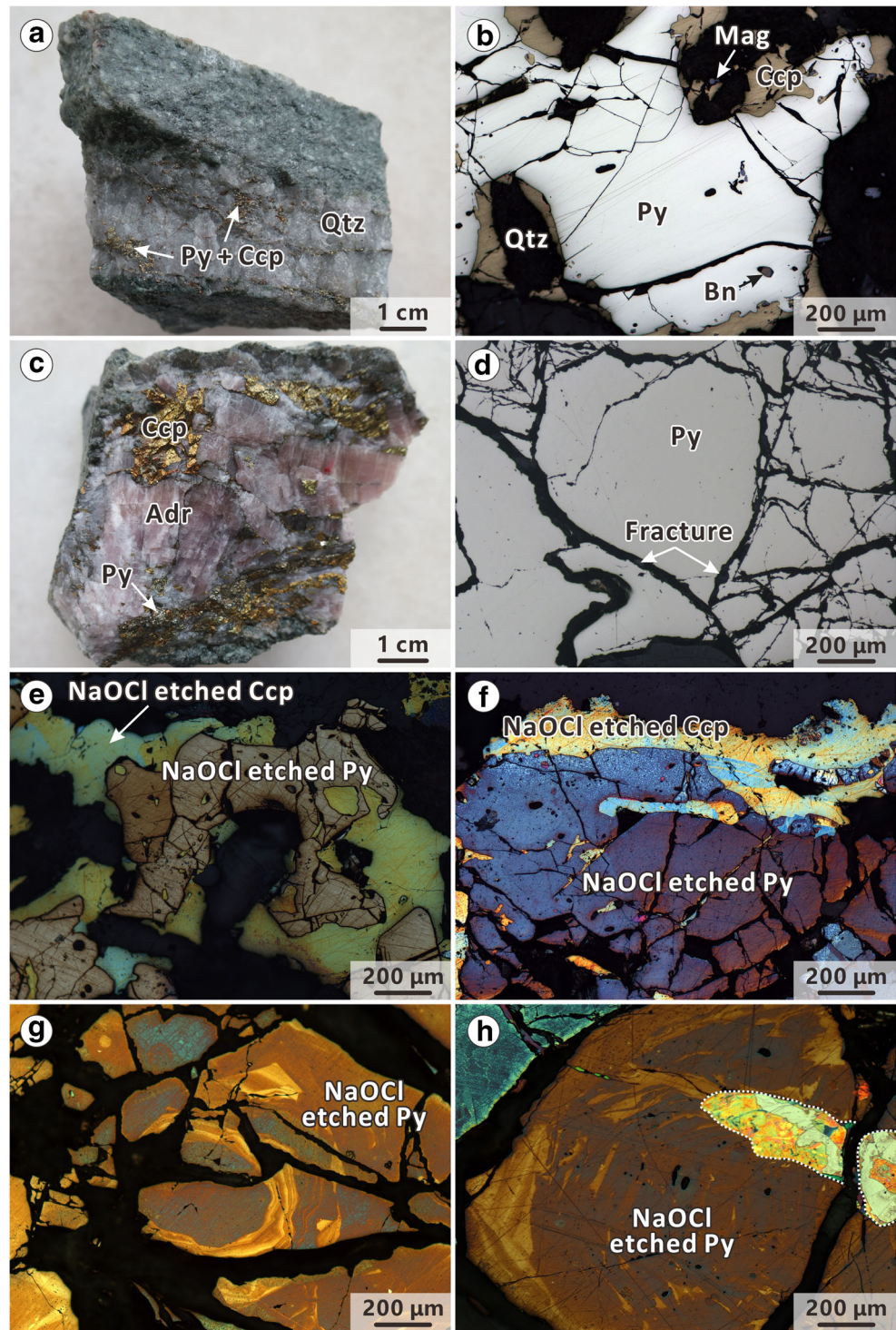
features or internal textures under reflected light (e.g., C281, Fig. 6b). Samples C233, C13, C311, C312, and C32 commonly include stage IIa veins 4–8 cm in width, and pyrite and chalcopyrite mainly occur as irregular masses in the vein (e.g., C32, Fig. 6c). Pyrite grains in the veins are cataclastic with abundant irregular thin fractures, and obvious multi-stage features and internal textures of pyrite grains have not been observed (e.g., C233, Fig. 6d).

To further investigate the differences between the pyrite in the stage Id veins and that in stage IIa veins and to determine whether they meet the necessary criteria for Re–Os isochron dating, pyrite grains from all nine samples were etched in NaOCl for 90 s, rinsed and then dried with pressurized air. This process can expose zoning, subgrain boundaries, and mineral inclusions under reflected light by tarnishing sulfide minerals (Sykora et al. 2018). Pyrite

samples etched with NaOCl from stage Id veins show variable colors, including brown (C281; Fig. 6e) and purple (C282; Fig. 6f), but they are homogeneous with no obvious internal textures. In contrast, pyrite from stage IIa veins shows obvious irregular zoning (e.g., C312 (Fig. 6g) and C32 (Fig. 6h)) with multi-stage pyrite and pyrite inclusions (e.g., C32, Fig. 6h). The zoning and multi-stage characteristics of pyrite in stage IIa veins suggest that they may have originated from multi-stage hydrothermal fluids (Huang et al. 2016). In addition, small amounts of molybdenite locally occur as coatings along stage IIa veins. The migration of ^{187}Os from molybdenite into sulfide coexisting with molybdenite can result in disturbed Re–Os isochron ages (Stein et al. 2003). Therefore, the stage IIa pyrite does not meet the necessary criteria for Re–Os isochron dating, and only the four pyrite samples from stage Id veins were chosen for Re–Os dating.

The analytical techniques for whole-rock geochemical analysis, whole-rock Sr–Nd isotopic analysis, zircon U–Pb–Hf, and trace element analysis as well as Re–Os analysis of pyrite are provided in ESM 3.

Results

Whole-rock geochemistry

Major, rare earth, and trace element compositions of three samples of the Lutopan quartz diorite porphyry are listed in ESM 4. The Lutopan quartz diorite porphyry samples have

SiO_2 contents ranging from 59 to 61 wt%. Their Al_2O_3 contents range from 16 to 17 wt%, FeO^T from 5.6 to 6.7 wt%, and CaO from 4.0 to 4.5 wt% (ESM 4). On alteration box plots (Large et al. 2001; Fig. 7), all samples plot in the least altered box, which is consistent with the low loss on ignition (LOI; 1.48 to 2.94 wt%) and petrographic observations (Fig. 3). As the geochemical effects of alteration on the samples are limited, they can be used to investigate the petrogenesis and geochemical characteristics of the mineralized intrusion at Atlas.

The three samples display similar rare-earth-element (REE) geochemistry, including light REE enrichment (ΣLREE = 79 to 90 ppm), heavy REE depletion (ΣHREE = 8.8 to 9.6 ppm), and listric-shaped normalized REE patterns with weak or absent Eu (Eu/Eu* = 1.00–1.07) and Ce anomalies (Ce/Ce* = 0.97–0.99; ESM 4 and Fig. 8a). The Lutopan quartz diorite porphyry is characterized by negative Nb, Ta, and Ti anomalies, with high-field-strength element (HFSE) depletion and large-ion lithophile element (LILE) enrichment (Fig. 8b).

Whole-rock Sr–Nd isotope data for the Lutopan stock are presented in ESM 4. The Sm, Nd, Rb, and Sr concentrations together with zircon U–Pb ages were used to calculate the initial isotope compositions at the time of magma crystallization to constrain the petrogenesis of the intrusions. All samples are characterized by relatively low initial I_{Sr} (initial $^{87}Sr/^{86}Sr$ ratio) ranging from 0.70373 to 0.70382 and $\varepsilon_{Nd}(t)$ values varying from 2.4 to 3.4. The samples have relatively homogeneous Nd
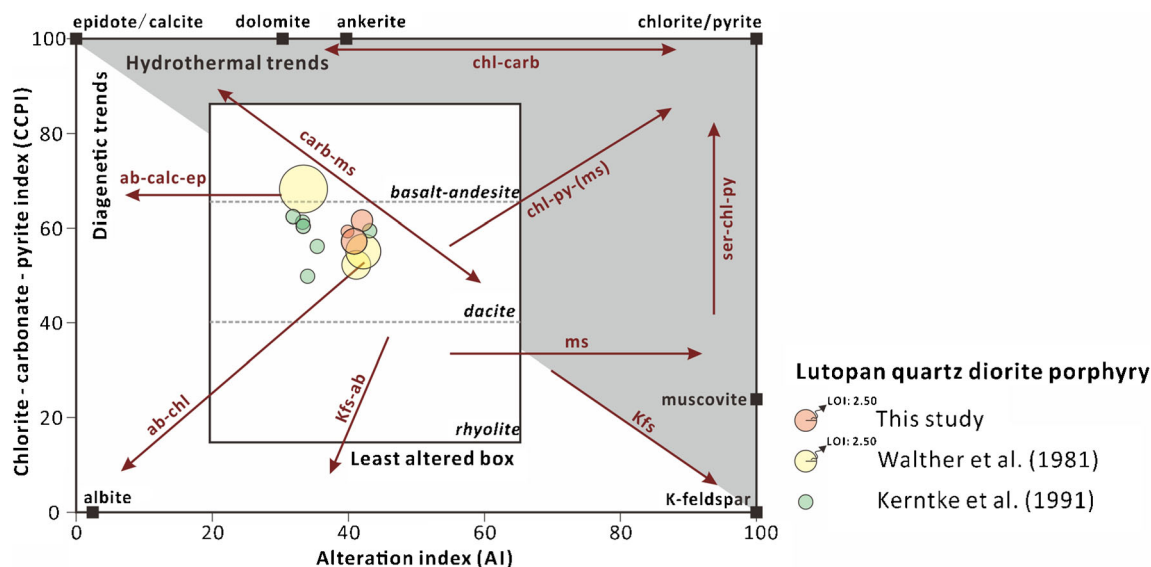

Fig. 7 Alteration box plots (after Large et al. 2001) showing that all samples from the Lutopan stock in this study have relatively weak hydrothermal alteration. Geochemical data for the Lutopan quartz diorite porphyry is from Walther et al. (1981) and Kerntke et al. (1991). AI = $100 \times (K_2O + MgO) / (K_2O + MgO + Na_2O + CaO)$; CCPI = $100 \times (MgO + FeO)/(MgO + FeO + K_2O + Na_2O)$. ab albite, calc calcite, carb carbonate, chl chlorite, ep epidote, Kfs K-feldspar, ms muscovite, py pyrite

Fig. 8 **a** Chondrite-normalized REE and **b** primitive-mantle-normalized diagrams for the Lutopan quartz diorite porphyry. Normalizing values are from Sun and McDonough (1989). Volcanic rock data from central Cebu Island is from Deng et al. (2015)
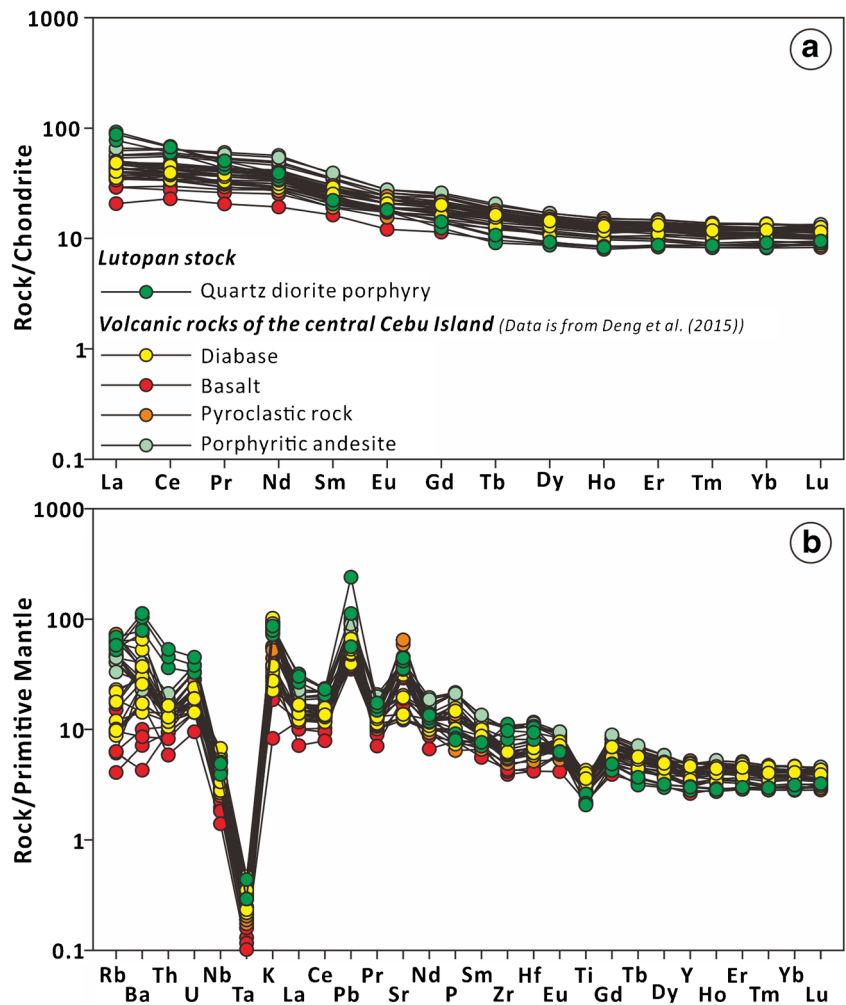
isotopic compositions with $^{143}Nd/^{144}Nd$ ratios ranging from 0.512706 to 0.512751, corresponding to T_{DM} of 589 to 726 Ma.

Zircon U–Pb dating and geochemistry

Zircon U–Pb isotope and trace element data are listed in ESMs 5 and 6. Cathodoluminescence (CL) images show that zircons from the Lutopan quartz diorite porphyry are generally euhedral and prismatic (100–200 μm long) and display oscillatory zoning (Fig. 9a). The zircons are characterized by LREE depletion, HREE enrichment, distinct positive Ce anomalies (Ce/Ce* ranging from 12 to 38), and negative Eu anomalies (Eu/Eu* = 0.40–0.62; ESM 6 and Fig. 9b), typical of igneous zircon (Hoskin and Schaltegger 2003; Zhao 2010). Twenty zircon grains yielded ages ranging from 115.7 to 103.2 Ma and a weighted mean age of 108.5 ± 1.6 Ma (MSWD =

0.81; ESM 5; Fig. 9c, d), close to the whole-rock Rb–Sr age of 107.6 ± 2.9 Ma (Walther et al. 1981).

The zircon Ce^{4+}/Ce^{3+} ratio and Ti-in-zircon thermometer can be used to determine the magma oxidation state and temperature at which zircons formed (Trotzsch and Ellis 2004, 2005; Watson and Harrison 2005; Liang et al. 2006), with the detailed calculations being presented in Ballard et al. (2002) and Ferry and Watson (2007). The oxygen fugacity (ΔFMQ) of the melt can be obtained based on the incorporation of cerium into zircon and the Ti-in-zircon temperature (Trail et al. 2011). In this study, the zircon Ce^{4+}/Ce^{3+} ratios, Ti-in-zircon thermometer, and ΔFMQ were calculated using Geo-fO_2 software (Li et al. 2019) with an assumed SiO_2 activity of 1 (all samples in this study contain primary magmatic quartz) and an activity of TiO_2 of 0.65 (Walker Jr. et al. 2013). The Ce^{4+}/Ce^{3+} ratios of the Lutopan quartz diorite porphyry range from 297 to
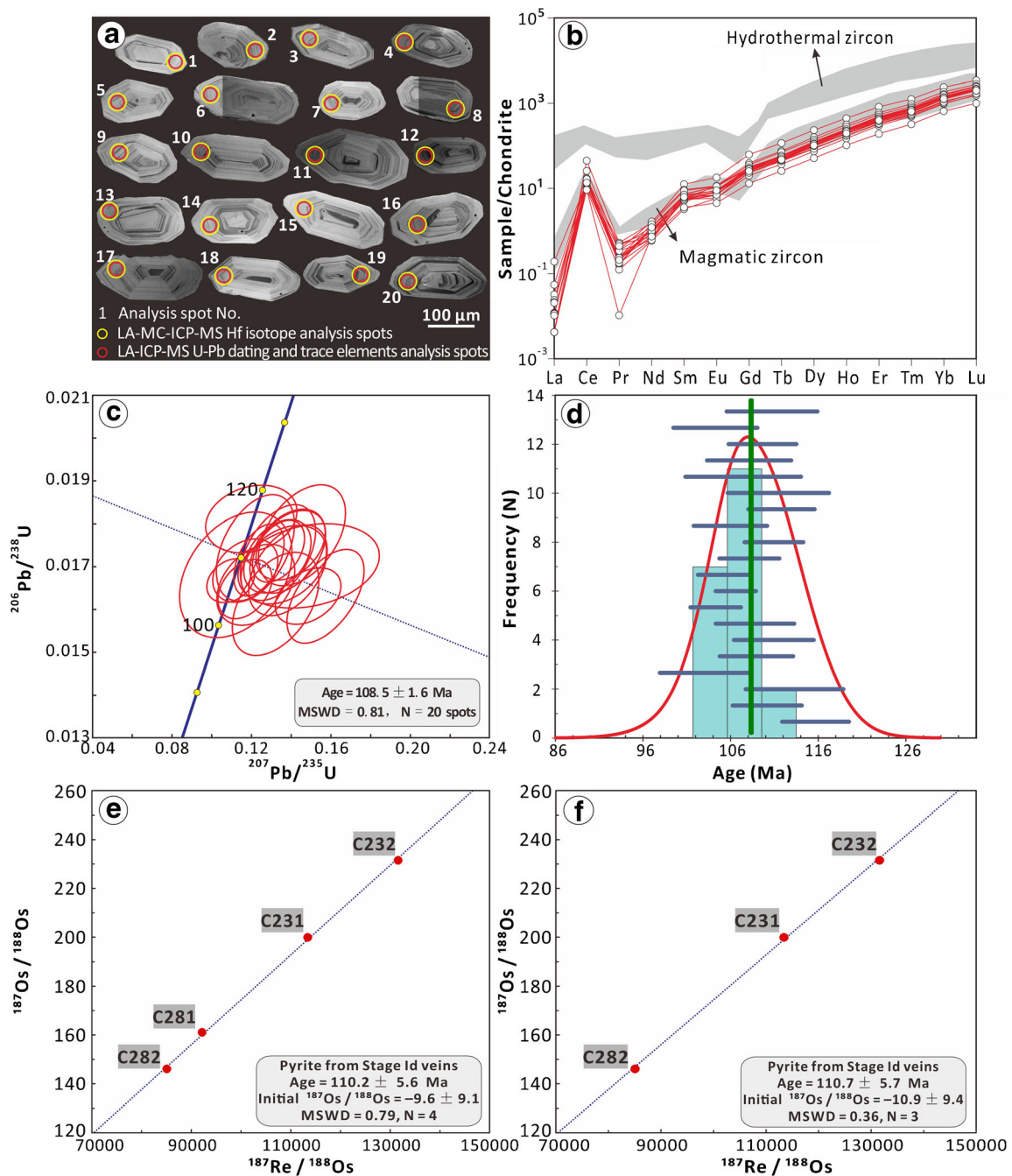
Fig. 9 a Representative zircon CL images with analyzed spots of the Lutopan quartz diorite porphyry. b Chondrite-normalized REE diagrams for zircon grains from the Lutopan quartz diorite porphyry. The average chondrite compositions are from Sun and McDonough (1989). c, d Zircon U–Pb concordia diagram and weighted mean $^{206}Pb/^{238}U$ ages for the quartz diorite porphyry from the Lutopan stock. Sample CPHI-

3's location: 10° 20′ 0.25″ N, 123° 43′ 46.58″ E, elevation = 89 m. e $^{187}Re/^{188}Os$ vs. $^{187}Os/^{188}Os$ plots for stage Id pyrite separates from samples of C281, C282, C231, and C232. f $^{187}Re/^{188}Os$ vs. $^{187}Os/^{188}Os$ plots for stage Id pyrite separates from samples of C282, C231, and C232 when excluding C281 which is over 800 m away from the other three samples. The locations of samples for Re–Os analysis are listed in ESM 2

668 (avg. 439), corresponding to calculated magma ΔFMQ of 1.3–4.4 (avg. 2.7), and a temperature range of 674 to 731 °C (avg. 706 °C; ESM 6).

Zircon Hf analyses were performed on the same grains as the U–Pb dating (Fig. 9a; ESM 7). The $\varepsilon_{Hf}(t)$ values of the Lutopan quartz diorite porphyry

are between 3.4 and 10.0 (avg. 7.3) with the two-stage Hf model ages ranging from 957 to 557 Ma.

Pyrite Re–Os dating

Total Re and Os abundances in pyrite from stage Id veins range from 74 to 85 ppb and 0.0840–0.0965 ppb, respectively, with $^{187}Re/^{188}Os$ ratios ranging from 85,081–131,614 and $^{187}Os/^{188}Os$ from 146.05–231.48 (ESM 8). The four samples have ^{192}Os contents ranging from 1.08 to 1.94 ppt with 95.18–96.90% of ^{187}Os in total Os, suggesting derivation from a similar source. The samples show a positive correlation with a coefficient of determination of 0.992 on a $^{187}Re/^{188}Os$ vs. $^{187}Os/^{188}Os$ diagram. Pyrite from stage Id veins yielded a well-defined Re–Os isochron age of 110.2 ± 5.6 Ma (MSWD = 0.79, initial $^{187}Os/^{188}Os$ ratio = − 9.6 ± 9.1; Fig. 9e). When sample C281, which is over 800 m away from the other samples, which are all within 200 m of each other, is excluded the other three samples yield a similar isochron age of 110.7 ± 5.7 Ma (MSWD = 0.36; Fig. 9f). Although the four samples were collected from different areas of the deposit they are all from the same vein stage and consequently can reasonably considered to be broadly coeval.

Discussion

Age of magmatism and mineralization

Given that the Atlas mineralization is mostly confined to the Lutopan stock (Divis 1983) and that the alteration typically show zoning around the stock (Divis 1983 and Sillitoe and Gappe 1984), the mineralization was likely genetically associated with the stock. The weighted mean zircon U–Pb age (108.5 ± 1.6 Ma) of the Lutopan quartz diorite porphyry is within error of the pyrite Re–Os age (110.2 ± 5.6 Ma) of stage Id veins, supporting a genetic relationship between the Lutopan stock and the Atlas mineralization. Additionally, the zircon U–Pb age of the Lutopan quartz diorite porphyry is younger than the volcanic rocks of the Cretaceous Cansi Formation in the area (126–117 Ma; Deng et al. 2015), consistent with the Lutopan stock intruding into the Cansi Formation (Divis 1983; Deng et al. 2015). The combined geochronology shows that the deposit formed in the Early Cretaceous (Albian), making it the only Mesozoic porphyry deposit recognized in the Philippines to date (Fig. 10; Braxton 2007). This conclusion supports the hypothesis that the early K–Ar age of 59.7 Ma by Wolfe (1972) of the Lutopan quartz diorite porphyry was the result of a superimposed thermal event corresponding to the Cenozoic magmatic activity in
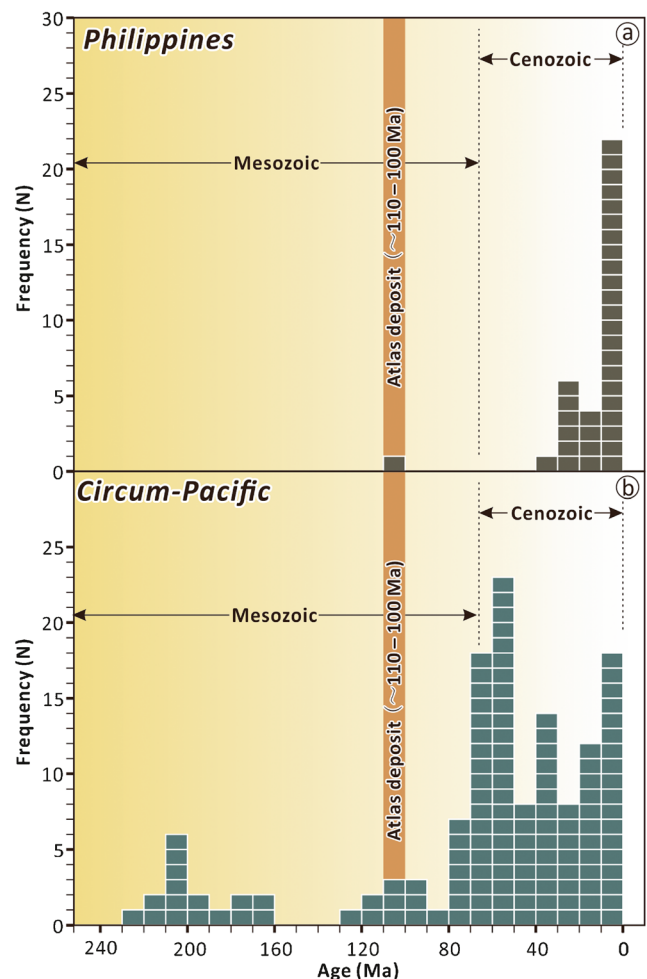

Fig. 10 a Ages of Philippine porphyry Cu–Au deposits, modified after Braxton (2007). **b** Ages of porphyry Cu–Au deposits from the circum-Pacific. Age data from Mutschler et al. (2010)

Cebu (Divis 1983) and rules out the Atlas mineralization age of ca. 61 Ma reported by Mutschler et al. (2010).

Geochemical potential for Cu mineralization

Many large porphyry Cu–Au deposits are associated with rocks with adakite-like affinity (Cooke et al. 2005; Richards 2009, 2011; Chiaradia et al. 2012; Loucks 2014). This is the case for many porphyry deposits in the Philippines (Sajona and Maury 1998) and is consistent with the close temporal and spatial relationship between mineralization at Atlas and the high-Mg adakite-like Lutopan stock.

Oxygen fugacity (fO_2) is a key factor that controls the formation of porphyry Cu deposits, and it is widely accepted that highly oxidized magmas favor porphyry Cu mineralization (Arculus 1994; Torrence and Compo 1998; Ballard et al. 2002; Sillitoe 2010; Shen et al. 2015; Sun et al. 2015; Zhang et al. 2017). Previous studies have suggested that an oxygen
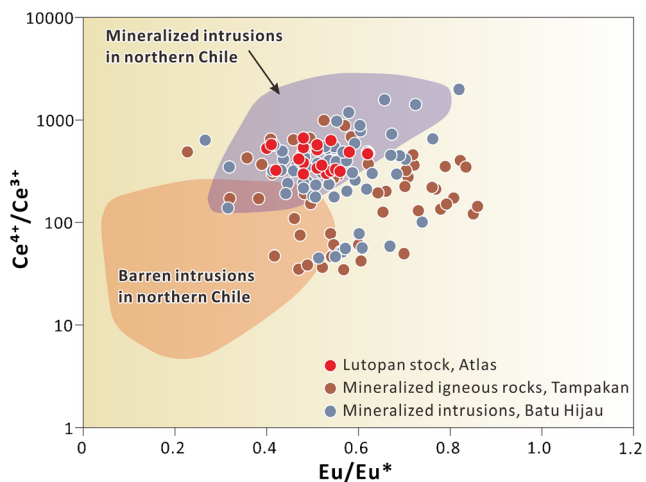
Fig. 11 Zircon Ce^{4+}/Ce^{3+} vs. Eu/Eu* plots for the Lutopan quartz diorite porphyry. Comparative data for mineralized and barren intrusions from northern Chile are from Ballard et al. (2002), Batu Hijau porphyry from Fiorentini and Garwin (2010) and Lu et al. (2016), and Tampakan from Rohrlach (2002) and Lu et al. (2016)

fugacity of > ΔFMQ + 2 (Mungall 2002; Sun et al. 2015) or + 1.5 (Zhang et al. 2017) is necessary for the generation of porphyry Cu deposits. The calculated ΔFMQ of the magma from the Lutopan stock ranges from 1.3 to 4.4 (avg. 2.7), with 17 of 20 zircon grains analyzed having oxygen fugacity > ΔFMQ + 1.5 (ESM 6). The highly oxidized composition of the Lutopan stock is consistent with high zircon Ce^{4+}/Ce^{3+} (297–668, avg. 439), indicating that it is favorable for the formation of porphyry Cu mineralization (Ballard et al. 2002; Trail et al. 2011). In addition to ΔFMQ and zircon Ce^{4+}/Ce^{3+}, zircon Eu anomalies can also indicate the fO_2 of the parental magmas (Ballard et al. 2002). Although both zircon Eu/Eu* and Ce^{4+}/Ce^{3+} are strongly dependent on melt REE concentrations, which are usually poorly constrained and controlled by the crystallization of titanite and other REE-bearing phases, zircon Eu/Eu* can broadly distinguish

between fertile and barren porphyry systems (Loader et al. 2017). For instance, mineralized intrusions in the Chuquicamata-El Abra porphyry Cu belt (northern Chile) have Eu/Eu* > 0.40 (Ballard et al. 2002), similar to the Lutopan zircon Eu anomalies (Fig. 11; Eu/Eu* = 0.40–0.62). On a zircon Ce^{4+}/Ce^{3+} vs. Eu/Eu* diagram (Fig. 11), the Lutopan quartz diorite porphyry plots with the northern Chilean mineralized intrusions (Ballard et al. 2002), mineralized igneous rocks from the Batu Hijau porphyry Cu–Au deposit (Sumbawa Island, Indonesia; Fiorentini and Garwin 2010; Lu et al. 2016), and the Tampakan porphyry Cu–Au deposit (Mindanao, Philippines; Rohrlach 2002; Lu et al. 2016).

High water contents in magma can suppress plagioclase fractionation (Moore and Carmichael 1998; Müntener et al. 2001; Richards et al. 2012; Loucks 2014) and promote early crystallization of garnet and amphibole (Alonso-Perez et al. 2009), resulting in high Sr contents at andesitic compositions (Defant and Drummond 1990). The presence of amphibole and biotite phenocrysts in the Lutopan porphyry suggests high magmatic water contents (≥ 4 wt% H_2O; Richards et al. 2012; Loucks 2014), consistent with the relatively low magmatic temperatures (Avg. Ti-in-zircon thermometry = 706 °C; ESM 6). This is further supported by the positive correlations between Al_2O_3/TiO_2 and V/Sc with SiO_2 (Fig. 12a, b). Previous studies have shown that whole-rock Al_2O_3/TiO_2 and V/Sc will increase with increasing SiO_2 during hydrous mafic-to-felsic magmatic differentiation, whereas these ratios remain constant or decline with rising SiO_2 during weakly hydrous or dry mafic-to-felsic magmatic differentiation (Loucks 2014). This combination of chemical features is consistent with the Lutopan intrusions being fertile for porphyry mineralization.
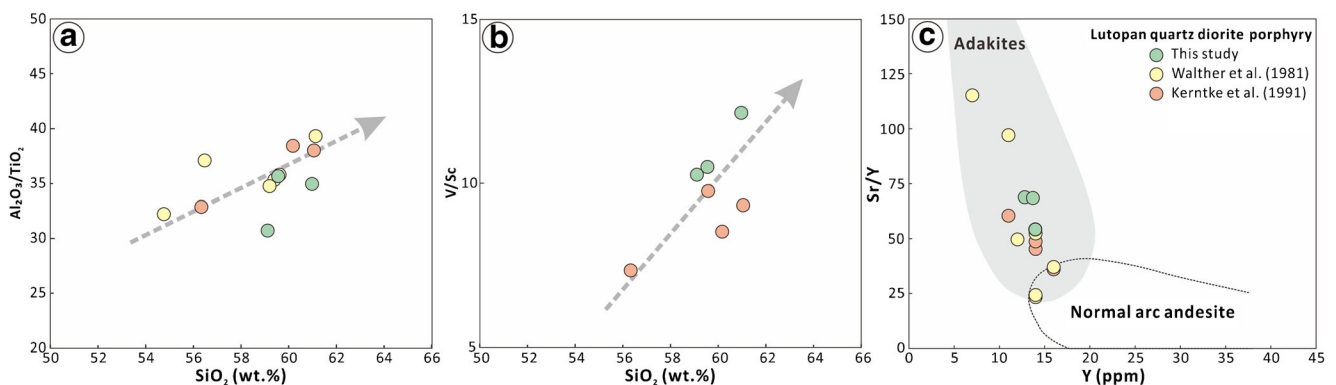

Fig. 12 Al_2O_3/TiO_2 vs. SiO_2 plots (**a**), V/Sc vs. SiO_2 plots (**b**), and Sr/Y vs. Y plots (**c**), for the Lutopan quartz diorite porphyry. Data are from this study, Walther et al. (1981), and Kerntke et al. (1991). Fields and limits for adakitic compositions from Richards and Kerrich (2007)

Petrogenesis of the Lutopan stock

The quartz diorite porphyry of the Lutopan stock has a composition consistent with the original definition of adakite that is characterized by ≥ 56 wt% SiO_2, ≥ 15 wt% Al_2O_3, low Y and Yb (≤ 18 and 1.9 ppm, respectively), and high Sr (≥ 400 ppm; Defant and Drummond 1990). Moreover, the quartz diorite porphyry has high Sr/Y ratios (54–69), and plots in the adakite field on a Sr/Y vs. Y diagram (Fig. 12c), an indication of adakite-like affinity. Previous studies have shown that adakite-like igneous rocks are widespread in the Philippines, especially in the Mankayan, Kalinga, Baguio, and Camarines Norte districts (Sajona et al. 1993, 1994; Jego et al. 2005). They were commonly interpreted to have formed as a result of the melting of the downgoing slab (Sajona and Maury 1998; Castillo et al. 1999; Yumul et al. 2000; Rae et al. 2004), and possibly linked with Cu–Au porphyry deposits (Thiéblemont et al. 1997; Sajona and Maury 1998; Rae et al. 2004). However, adakite-like rocks in arc environments can also be generated by other magmatic processes, including (1) partial melting of lower crustal garnet amphibolites or eclogites (e.g., Conrey et al. 2001; Saleeby et al. 2003; Tulloch and Kimbrough 2003; Richards and Kerrich 2007), (2) interaction between asthenospheric melts and lower crust (e.g., Gromet and Silver 1983; Feeley and Hacker 1995; Klepeis et al. 2003; Tulloch and Kimbrough 2003; Richards 2002; Richards and Kerrich 2007), and (3) fractional crystallization of minerals that preferentially partition Y and HREE (esp., amphibole and garnet) in the absence of significant plagioclase

fractionation (e.g., Castillo et al. 1999; Richards 2002; Richards and Kerrich 2007).

Zircon Hf and whole-rock Sr–Nd isotope compositions can be used to investigate possible magma sources (Woodhead et al. 2001; Kemp et al. 2007; Hollings et al. 2011a). The $\varepsilon_{Hf}(t)$ values of the quartz diorite porphyry range from 3.4 to 10.0 (ESM 7) and are slightly lower than those of the Early Cretaceous volcanic suite on Cebu Island (Fig. 13a; Deng et al. 2015). The Sr–Nd isotopic data for the Atlas district lie along the mantle array and show less depletion than MORB and adakite-like rocks derived from slab melts in the Baguio district, Philippines (Polve et al. 2007; Hollings et al. 2011a, b; Fig. 13b). Consequently, a depleted mantle or young lower continental crust source is proposed for the Lutopan stock, consistent with its relatively high Mg numbers (49–53; ESM 4), but inconsistent with the slab melt model for the petrogenesis of adakites. Given the ability to fractionate HREEs and the stability of garnet, partial melting of both subducting oceanic crust under eclogite facies conditions and lower crustal garnet amphibolites or eclogites can lead to high La/Yb ratios (≥ 20; Richards 2011). The relatively low La/Yb ratios (9–11; ESM 4) of the Lutopan stock and the zircon difference between two-stage Hf model ages (957–557 Ma) and $^{206}U/^{238}Pb$ ages (115.7–103.2 Ma) is not consistent with partial melting of young and hot oceanic crust (< 25 m.y. old; Defant and Drummond 1990). This suggests that the Lutopan stock may have been derived from partial melting of young lower continental crust or interaction between asthenospheric melts and
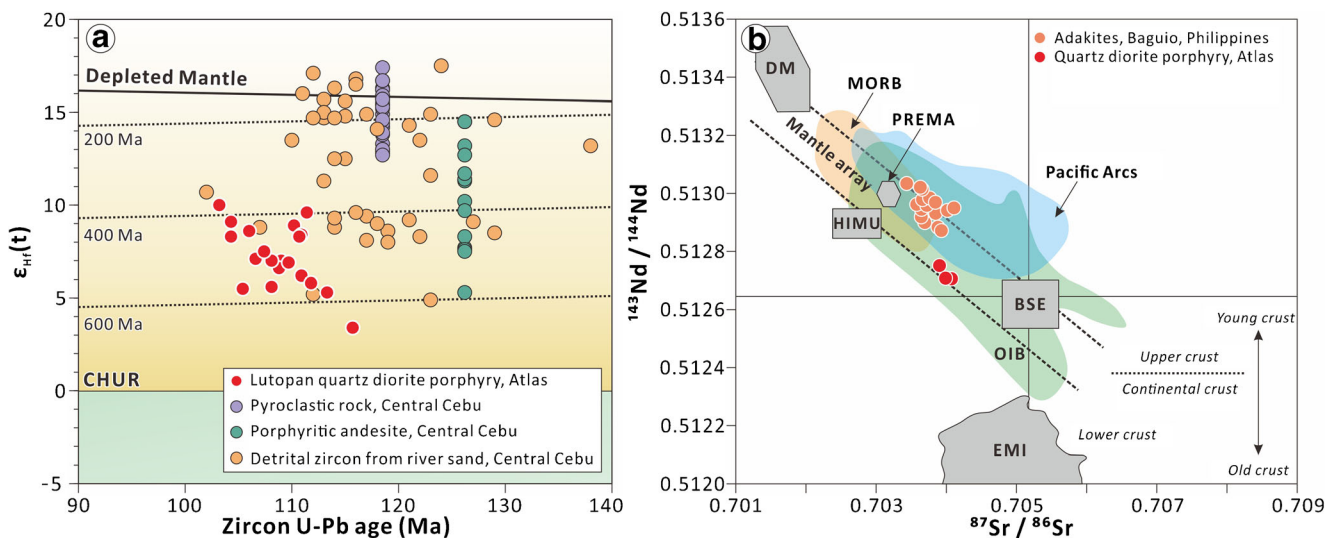

Fig. 13 **a** Relationships between $\varepsilon_{Hf}(t)$ values and U–Pb ages for zircon grains from the Lutopan quartz diorite porphyry. Data are from this study and Deng et al. (2015). **b** $^{143}Nd/^{144}Nd$ vs. $^{87}Sr/^{86}Sr$ diagram for the Lutopan quartz diorite porphyry. Data from the Baguio district,

Philippines, are from Polve et al. (2007) and Hollings et al. (2011a, b). DM depleted mantle, BSE bulk silicate Earth, EMI and EMII enriched mantle, HIMU mantle with high U/Pb ratio, PREMA frequently observed prevalent mantle composition

young lower crust, and the adakite-like geochemical composition of the stock is probably not the result of partial melting of either oceanic crust or lower crustal garnet amphibolites or eclogites.

High magmatic water contents commonly cause abundant amphibole (± garnet) fractionation but suppression of plagioclase crystallization (Richards 2011). Amphibole and garnet preferentially partition HREE, and their fractionation will generate magmas with increasing Sr/Y ratios to adakite-like trace element compositions (e.g., Castillo et al. 1999; Richards 2002; Richards and Kerrich 2007). Abundant amphibole phenocrysts and high magmatic water contents suggest that amphibole and/or garnet fractionation played a role in the petrogenesis of the Lutopan stock. The porphyry shows listric-shaped normalized REE patterns with weak or absent Eu anomalies (Fig. 8a), indicating the fractionation of amphibole, rather than garnet (Richards 2011). Moreover, the positive correlations between Al_2O_3/TiO_2 and V/Sc with SiO_2 are also consistent with fractionation (Fig. 12a, b). Therefore, we propose that the quartz diorite porphyry may have evolved to adakite-like trace element compositions through amphibole fractionation.

Tectonic and exploration implications

Previous studies have shown that the Cenozoic tectonic setting of the Philippine archipelago is characterized by a number of arc systems (Hall 1996, 2002; Pubellier et al. 2003; Yumul 2007; Yumul et al. 2008). However, the Mesozoic tectonic setting is poorly constrained because the paleomagnetic, petrologic, geochemical, and geochronological data for Mesozoic rocks in the Philippines are generally lacking (Hall 1996; Deng et al. 2015).

At ca. 120–100 Ma, a "superplume" was generated by convection through the entire mantle and erupted beneath the mid-Cretaceous Pacific basin, which caused peak production rates of oceanic crust (Larson 1991) and increased ridge-push force at subduction zones (Vaughan 1995). This event was coeval with the formation of porphyry deposits during the Early Cretaceous in the circum-Pacific regions (Fig. 10b; Mutschler et al. 2010). Given the similarity in age, it is possible that the Atlas deposit also formed at least in part as a result of this event. The Philippine Mobile Belt is believed to have formed as an intra-oceanic island arc related to the subduction of the Philippine Sea and/or Pacific plates (Rangin et al. 1990), likely in the southern Pacific, or at the boundary between the Pacific and North New Guinea Basin in the Late Cretaceous (Maruyama et al. 1989; Deng et al. 2015) and was translated northwestward and rotated clockwise in the Cenozoic to the present-day location, with the collision between the Palawan micro-continental block and the Philippine Mobile Belt (Hall 1996, 2002). The New Guinea Basin opened as a back-arc basin related to the subduction of the paleo-Pacific plate, along the northern margin of Australia during the Middle

Jurassic–Early Cretaceous (Monnier et al. 1995; Pubellier et al. 2003). The peak in the subduction of the paleo-Pacific plate toward the Eurasian continent and India-Australia plate occurred during the Cretaceous (Zhou et al. 2008), coeval with the Pacific Superplume.

The pronounced depletion of HFSEs and enrichment in LILEs (Fig. 8b) suggest that the Lutopan quartz diorite porphyry formed above a subduction zone. The widespread 126–117 Ma normal arc volcanic suites on Cebu Island have been linked to the subduction of the paleo-Pacific plate beneath the proto-Philippine Sea plate and/or India-Australia plate (Deng et al. 2015). Therefore, the Early Cretaceous Lutopan quartz diorite porphyry and associated giant Cu–Au mineralization is likely related to the subduction of the paleo-Pacific plate beneath the proto-Philippine Sea plate and/or India-Australia plate.

Although isolated areas of Cretaceous arc rocks have been documented farther north in the Philippines on Catanduanes Island and in southeastern Luzon on Rapu Rapu Island (Dimalanta and Yumul 2004), Cretaceous igneous rocks (quartz diorite intrusions and andesitic rocks) in the Philippines are primarily exposed on both Cebu and Bohol islands (Fig. 1) and occur in a northwest-trending belt extending from southeastern Bohol to the central highlands of Cebu (Hammarstrom et al. 2010). Except for the Atlas deposit, only the Balak-5 porphyry copper deposit (5 Mt at 0.80% Cu; Hammarstrom et al. 2010) in northern Bohol has been recognized within this belt. The pyrite Re–Os isochron ages (110.2 ± 5.6 Ma of stage Id veins) of the Atlas deposit, the high oxygen fugacity and H_2O concentrations and low magmatic temperatures of the magma corresponding to the Lutopan stock, and the occurrence of the Balak-5 porphyry deposit demonstrate the potential of this Cretaceous igneous belt for porphyry copper mineralization. Given that porphyry Cu deposits commonly form clusters or belts, which may be derived from the same deep-seated magma chamber (Cooke et al. 2014) and that the uplift of the horst resulted in the erosion of the sedimentary cover and facilitated the discovery of the Atlas deposit (Madamba 1972; Divis 1983), we suggest that the northwest-trending Cretaceous Cebu–Bohol igneous belt is a prospective area for Mesozoic porphyry Cu deposits in the Philippines.

Conclusions

The Atlas Cu–Au deposit is intimately related, both spatially and temporally, to the multi-phase adakite-like quartz diorite porphyry of the Lutopan stock which was emplaced at 108.5 ± 1.6 Ma (U–Pb on zircon) and produced mineralization which has been dated at 110.2 ± 5.6 Ma (Re–Os on pyrite). The magma for the Lutopan stock formed under conditions of high oxygen fugacity, high H_2O concentration and low magmatic temperatures, favorable for copper–gold mineralization. The depleted mantle or young lower continental crust source

suggested by the zircon $\varepsilon_{Hf}(t)$ values, the whole-rock Sr–Nd isotopic data and La/Yb ratio indicate that the Lutopan quartz diorite porphyry was likely derived from partial melting of young lower continental crust or interaction between asthenospheric melts and lower crust melts, and subsequently evolved to adakite-like trace element compositions through amphibole fractionation. These processes were probably linked to the subduction of the paleo-Pacific plate beneath the proto-Philippine Sea plate and/or India-Australia plate in the Early Cretaceous. The occurrence of Atlas and its intimate association with the adakite-like quartz diorite porphyry suggest that the belt may be prospective for Cretaceous porphyry Cu–Au deposits.

References

Alonso-Perez R, Müntener O, Ulmer P (2009) Igneous garnet and amphibole fractionation in the roots of island arcs: experimental constraints on andesitic liquids. Contrib Mineral Petrol 157:541–558

Arculus RJ (1994) Aspects of magma genesis in arcs. Lithos 33:189–208

Arribas AJ, Hedenquist JW, Itaya T, Okada T, Concepcion RA, Garcia JS (1995) Contemporaneous formation of adjacent porphyry and epithermal Cu-Au deposits over 300 ka in northern Luzon Philippines. Geology 23:337–340

Aurelio MA (2000) Shear partitioning in the Philippines: constraints from Philippine Fault and global positioning system data. Island Arc 9:584–597

Aurelio MA, Peña RE (2002) Geology and mineral resources of the Philippines. Manila, Department of Environment and Natural Resources-Mines and Geosciences Bureau, vol 391

Aurelio MA, Peña RE, Taguibao KJL (2013) Sculpting the Philippine archipelago since the Cretaceous through rifting, oceanic spreading, subduction, obduction, collision and strike–slip faulting: contribution to IGMA5000. J Asian Earth Sci 72:102–107

Ballard JR, Michael P, Campbell HI (2002) Relative oxidation states of magmas inferred from Ce(IV)/Ce(III) in zircon: application to porphyry copper deposits of northern Chile. Contrib Mineral Petrol 144:347–364

Balce GR (1980) Geology of the Baguio district and its implication on the tectonic development of the Luzon Central Cordillera. Geology & Paleontology of Southeast Asia 21:265–287

Braxton DP (2007) Boyongan and Bayugo porphyry copper-gold deposits NE Mindanao, Philippines: geology, geochemistry, and tectonic evolution: Ph.D. thesis. University of Tasmania

Braxton DP, Cooke DR, Ignacio AM, Rye RO, Waters PJ (2009) Ultra-deep oxidation and exotic copper formation at the late Pliocene Boyongan and Bayugo porphyry copper-gold deposits, Surigao, Philippines: geology, mineralogy, paleoaltimetry, and their implications for geologic, physiographic, and tectonic controls. Econ Geol 104:333–349

Braxton DP, Mathur R (2011) Exploration applications of copper isotopes in the supergene environment: a case study of the Bayugo porphyry copper-gold deposit, southern Philippines. Econ Geol 106:1447–1463

Braxton DP, Cooke DR, Dunlap J, Norman M, Reiners P, Stein H, Waters P (2012) From crucible to graben in 2.3 Ma: a high-resolution geochronological study of porphyry life cycles, Boyongan-Bayugo copper-gold deposits, Philippines. Geology 40:471–474

Braxton DP, Cooke DR, Ignacio AM, Waters PJ (2018) Geology of the Boyongan and Bayugo porphyry Cu-Au deposits: an emerging porphyry district in Northeast Mindanao, Philippines. Econ Geol 113:83–131

Cao MJ, Hollings P, Cooke DR, Evans NJ, McInnes BIA, Qin KZ, Li GM, Sweet G, Baker M (2018) Physicochemical processes in the magma chamber under the Black Mountain porphyry cu-au deposit, Philippines: insights from mineral chemistry and implications for mineralization. Econ Geol 113:63–82

Castillo PR, Janney PE, Solidum RU (1999) Petrology and geochemistry of Camiguin Island, southern Philippines: insights to the source of adakites and other lavas in a complex arc setting. Contrib Mineral Petrol 134:33–51

Chiaradia M, Ulianov A, Kouzmanov K, Beate B (2012) Why large porphyry Cu deposits like high Sr/Y magmas. Sci Rep 2:685

Cooke DR, Hollings P, Walsh JL (2005) Giant porphyry deposits: characteristics, distribution, and tectonic controls. Econ Geol 100:801–818

Cooke DR, Deyell-Wurst C, Waters PJ, Gonzales RI, Zaw K (2011) Evidence for magmatic-hydrothermal fluids and ore-forming processes in epithermal and porphyry deposits of the Baguio district, Philippines. Econ Geol 106:1399–1424

Cooke DR, Hollings P, Wilkinson JJ, Tosdal RM (2014) Geochemistry of porphyry deposits. In: Holland HD, Turekian KK (eds) Treatise on geochemistry, 2nd section 13. Elsevier, Oxford, pp 357–381

Conrey RM, Hooper PR, Larson PB, Chesley J, Ruiz J (2001) Trace element and isotopic evidence for two types of crustal melting beneath a high cascade volcanic center, Mt. Jefferson, Oregon. Contrib Mineral Petrol 141:710–732

Defant MJ, Drummond MS (1990) Derivation of some modern arc magmas by melting of young subducted lithosphere. Nature 347: 662–665

Deng JH, Yang XY, Zhang ZF, Santosh M (2015) Early Cretaceous arc volcanic suite in Cebu Island, Central Philippines and its implications on paleo-Pacific plate subduction: constraints from geochemistry, zircon U–Pb geochronology and Lu–Hf isotopes. Lithos 230:166–179

Dimalanta CB, Suerte LO, Yumul GP, Tamayo RA, Ramos EGL (2006) A Cretaceous supra-subduction oceanic basin source for central Philippine ophiolitic basement complexes: geological and geophysical constraints. Geosci J 10:305–320

Dimalanta CB, Yumul GP (2004) Crustal thickening in an active margin setting (Philippines)—the whys and the hows. Episodes 27:260–264

Divis AF (1983) The geology and geochemistry of Philippine porphyry copper deposits. In: Hayes DE (ed) The tectonic and geologic evolution of Southeast Asian seas and islands—part, vol 2. American Geophysical Union, Washington, D.C., pp 173–216

Faure M, Marchadier Y, Rangin C (1989) Pre-Eocene synmetamorphic structure in the Mindoro-Romblon-Palawan area, West Philippines, and implications for the history of Southeast-Asia. Tectonics 8:963–979

Feeley TC, Hacker MD (1995) Intracrustal derivation of Na-rich andesitic and dacitic magmas: an example from Volcán Ollagüe, Andean Central volcanic zone. J Geol 103:213–225

Fernandez JC (1981) Geology and mineral resources of the Philippines. Manila, Philippines, Bureau of Mines and Geosciences, Ministry of Natural Resources, 406 p

Ferry JM, Watson EB (2007) New thermodynamic models and revised calibrations for the Ti-in-zircon and Zr-in-rutile thermometers. Contrib Mineral Petrol 154:429–437

Fiorentini ML, Garwin SL (2010) Evidence of a mantle contribution in the genesis of magmatic rocks from the Neogene Batu Hijau district in the Sunda Arc, South Western Sumbawa, Indonesia. Contrib Mineral Petrol 159:819–837

Gromet LP, Silver LT (1983) Rare earth element distributions among minerals in a granodiorite and their petrogenetic implications. Geochim Cosmochim Acta 47:925–939

Hall R (1996) Reconstructing Cenozoic SE Asia, in Hall, R., Blundell, D.J., (eds.), Tectonic evolution of Southeast Asia: Geological Society Special Publications 106: 153–184

Hall R (2002) Cenozoic geological and plate tectonic evolution of SE Asia and the SW Pacific: computer-based reconstructions, model and animations. J Asian Earth Sci 20:353–431

Hammarstrom JM, Bookstrom AA, Dicken CL, Ludington S, Jr GRR, Zientek ML (2010) Appendix I. Porphyry copper assessment for tract 142pCu7306, Bohol-Cebu area—Philippines. In: Porphyry copper assessment of East and Southeast Asia—Philippines, Taiwan (Republic of China), Republic of Korea (South Korea), and Japan: U.S. Department of the Interior and U.S. Geological Survey: 167–179

Hedenquist JW, Arribas A, Reynolds TJ (1998) Evolution of an intrusion-centered hydrothermal system: far Southeast-Lepanto porphyry and epithermal Cu-Au deposits, Philippines. Econ Geol 93:373–404

Hollings P, Cooke DR, Waters PJ, Cousens B (2011a) Igneous geochemistry of mineralized rocks of the Baguio district, Philippines: implications for tectonic evolution and the genesis of porphyry-style mineralization. Econ Geol 106:1317–1333

Hollings P, Wolfe R, Cooke DR, Waters PJ (2011b) Geochemistry of Tertiary igneous rocks of northern Luzon, Philippines: evidence for a back-arc setting for alkali porphyry copper-gold deposits and a case for slab roll-back. Econ Geol 106:1257–1277

Hollings P, Sweet G, Baker M, Cooke D, Fiedman R (2013) Tectonomagmatic controls on porphyry mineralization: geochemical evidence from the Black Mountain porphyry system, Philippines. In: Colporn, M., Bissig, T., Rusk, B.G., Thompson, J.F.H. (Eds.), Tectonics, metallogeny, and discovery: the North American Cordillera and similar accretionary settings: Society of Economic Geologists, Special Publication 17: 301–335

Hoskin PWO, Schaltegger U (2003) The composition of zircon and igneous and metamorphic petrogenesis. Rev Mineral Geochem 53:27–62

Huang XW, Qi L, Gao JF, Meng YM (2016) Some thoughts on sulfide Re-Os isotope dating: bulletin of mineralogy. Petrology and Geochemistry 35:432–440 **in Chinese with English abstract**

Jego S, Maury RC, Polvé M, Yumul, Herve Bellon GP, Tamayo RA, Cotten J (2005) Geochemistry of Adakites from the Philippines: constraints on their origins. Resour Geol 55(3):163–188

Kemp AIS, Hawkesworth CJ, Foster GL, Paterson BA, Woodhead JD, Hergt JM, Gray CM, Whitehouse MJ (2007) Magmatic and crustal differentiation history of granitic rocks from hafnium and oxygen isotopes in zircon. Science 315:980–983

Kerntke M, Tarkian M, Baumann A (1991) Geochemie und geochronologie der magmatite von Lutopan und Talamban, Cebu (Philippinen). Mitteilungen aus dem Geologisch-Palaeontologischen Institut der Universitaet Hamburg 71:93–120 (in German)

Kesler SE (1997) Metallogenic evolution of convergent margins: selected ore deposit models. Ore Geol Rev 12:153–171

Klepeis KA, Clarke GL, Rushmer T (2003) Magma transport and coupling between deformation and magmatism in the continental lithosphere. GSA Today 13:4–11

Large RR, Gemmell JB, Paulick H, Huston D (2001) The alteration box plot: a simple approach to understanding the relationships between alteration mineralogy and lithogeochemistry associated with volcanichosted massive sulfde deposits. Econ Geol 96:957–971

Larson RL (1991) Latest pulse of Earth: Evidence for a mid-Cretaceous superplume. Geology 19(6):547–550

Li W, Cheng Y, Yang Z (2019) Geo-fO_2: integrated software for analysis of magmatic oxygen fugacity. Geochem Geophys Geosyst. https://doi.org/10.1029/2019GC008273

Liang HY, Campell HI, Allen C, Sun WD, Liu CQ, Yu HX, Xie YW, Zhang YQ (2006) Zircon Ce^{4+}/Ce^{3+} ratios and ages for Yulong ore-bearing porphyries in eastern Tibet. Mineral Deposita 41:152–159

Loader MA, Wilkinson JJ, Armstong RN (2017) The effect of titanite crystallisation on Eu and Ce anomalies in zircon and its implications for the assessment of porphyry Cu deposit fertility. Earth Planet Sci Lett 472:107–119

Loucks RR (2014) Distinctive composition of copper–ore-forming arc magmas. Aust J Earth Sci 61:5–16

Lu YJ, Loucks RR, Fiorentini M, McCuaig C, Evans NJ, Yang ZM, Hou ZQ, Kirkland CL, Parra-Avila LA, Kobussen A (2016) Zircon compositions as a pathfinder for porphyry $Cu \pm Mo \pm Au$ deposits. Econ Geol 19:329–347

Madamba FA (1972) Geology and mineralization of the Atlas copper deposits in Cebu Island, Philippines. Journal of the Geological Society of the Philippines 26:13–24

Maruyama S, Liou JG, Seno T (1989) Mesozoic and Cenozoic evolution of Asia. In: BenAvraham Z (ed.) The evolution of the pacific ocean margins. Oxford University Press, New York, pp 75–99

Monnier C, Girardeau J, Maury RC, Cotten J (1995) Back-arc basin origin for the East Sulawesi ophiolite (Eastern Indonesia). Geology 23:851–854

Moore GM, Carmichael ISE (1998) The hydrous phase equilibria (to 3 kbar) of an andesite and basaltic andesite from western Mexico: constraints on water content and conditions of phenocryst growth. Contrib Mineral Petrol 130:304–319

Mungall JE (2002) Roasting the mantle: slab melting and the genesis of major Au and Au-rich Cu deposits. Geology 30:915–918

Mutschler FE, Ludington S, Bookstrom AA (2010) Giant porphyry related metal camps of the world — a database. USGS open-file report, pp 99–556 (6 pp. (http://geopubs.wr.usgs.gov/open-file/of99-556/))

Müntener O, Kelemen PB, Grove TL (2001) The role of H_2O during crystallization of primitive arc magmas under uppermost mantle conditions and genesis of igneous pyroxenites: an experimental study. Contrib Mineral Petrol 141:643–658

Ozawa A, Tagami T, Listanco EL, Arpa CB, Sudo M (2004) Initiation and propagation of subduction along the Philippine trench: evidence from the temporal and spatial distribution of volcanoes. J Asian Earth Sci 23:105–111

Philippine Bureau of Mines and Geosciences (1986) Geology and mineral resources of the Philippines, v. 2—Mineral resources: Philippine Bureau of Mines and Geosciences, 446 p

Polve M, Maury RC, Jego S, Bellon H, Margoum A, Yumul GP, Payot BD, Tamayo RA, Cotten J (2007) Temporal geochemical evolution of Neogene magmatism in the Baguio gold–copper mining district (northern Luzon, Philippines). Resour Geol 57:197–218

Pubellier M, Ali J, Monnier C (2003) Cenozoic plate interaction of the Australia and Philippine Sea plates: "hit-and-run" tectonics. Tectonophysics 363:181–199

Rae AJ, Cooke DR, Phillips D, Zaide-Delfin M (2004) The nature of magmatism at Palinpinon geothermal field, Negros island, Philippines: implications for geothermal activity and regional tectonics. J Volcanol Geotherm Res 129:321–342

Rangin C, Jolivet L, Pubellier M (1990) A simple model for the tectonic evolution of Southeast Asia and Indonesian region for the past 43 My. Bulletin of the Geological Society of France 8:889–905

Rangin C, Le Pichon X, Mazzotti S, Pubellier M, Chamotrooke N, Aurelio M, Walpersdorf A, Quebral R (1999) Plate convergence measured by GPS across the Sundaland/Philippine sea plate deformed boundary: the Philippines and eastern Indonesia. Geophys J Int 139:296–316

Richards JP (2002) Discussion on "Giant versus small porphyry copper deposits of Cenozoic age in northern Chile: adakitic versus normal calc-alkaline magmatism" by Oyarzun et al. (Mineralium Deposita 36:794–798, 2001). Mineral Deposita 37:1–26

Richards JP (2009) Postsubduction porphyry Cu-Au and epithermal Au deposits: products of remelting of subduction-modified lithosphere. Geology 37:247–250

Richards JP (2011) Magmatic to hydrothermal metal fluxes in convergent and collided margins. Ore Geol Rev 40: 911–916, 1

Richards JP (2013a) Giant ore deposits formed by optimal alignments and combinations of geological processes. Nat Geosci 6:911–916

Richards JP (2013b) High Sr/Y arc magmas and porphyry Cu ± Mo ± Au deposits: just add water. Econ Geol 106:1075–1081

Richards JP, Kerrich R (2007) Adakite-like rocks: their diverse origins and questionable role in metallogenesis. Econ Geol 102:537–576

Richards JP, Spell T, Rameh E, Razique A, Fletcher T (2012) High Sr/Y magmas reflect arc maturity, high magmatic water content, and porphyry Cu ± Mo ± Au potential: examples from the Tethyan arcs of central and eastern Iran and western Pakistan. Econ Geol 107:295–332

Rohrlach BD (2002) Tectonic evolution, petrochemistry, geochronology and palaeohydrology of the Tampakan porphyry and high sulphidation epithermal Cu-Au deposit Mindanao, Philippines: Ph.D. thesis. The Australian National University

Sajona F, Maury R (1998) Association of adakites with gold and copper mineralization in the Philippines. Comptes Rendus Academy Science Paris Sciences de la Terre et des Planetes 326:27–34

Sajona F, Maury R, Bellon H, Cotton J, Pubelier M, Rangin C (1993) Initiation of subduction and the generation of slab melts in western and eastern Mindanao, Philippines. Geology 21: 1007–1010

Sajona F, Bellon H, Maury R, Pubelier M, Cotton J, Rangin C (1994) Magmatic response to abrupt changes in tectonic setting: Pliocene Quaternary calc-alkaline lavas and Nb-enriched basalts of Leyte and Mindanao (Philippines). Tectonophysics 237:47–72

Saleeby J, Ducea M, Clemens-Knott D (2003) Production and loss of high-density batholithic root, southern Sierra Nevada, California. Tectonics 22:1064

Shen P, Hattori K, Pan H, Jackson S, Seitmuratova E (2015) Oxidation condition and metal fertility of granitic magmas: zircon trace-element data from porphyry Cu deposits in the Central Asian Orogenic Belt. Econ Geol 110:1861–1878

Shinohara H, Hedenquist JW (1997) Constraints on magma degassing beneath the far southeast porphyry Cu-Au deposit, Philippines. J Petrol 38:1741–1752

Sillitoe RH (2000) Styles of high-sulphidation gold, silver and copper mineralization in porphyry and epithermal environments. The Australasian Institute of Mining and Metallurgy Proceedings 305:19–34

Sillitoe RH (2010) Porphyry copper systems. Econ Geol 105:3–41

Sillitoe RH, Gappe IM (1984) Philippine porphyry copper deposits: geologic setting and characteristics. CCOP-ESCAP Technical Publication 14 **89 p**

Singer DA, Berger VI, Moring BC (2008) Porphyry copper deposits of the World—Database and grade and tonnage models, 2008: U.S. Geological Survey Open-File Report 2008–1155, accessed June 1, 2011, at http://pubs.usgs.gov/of/2008/1155/

Smoliar MI, Walker RJ, Morgan JW (1996) Re–Os ages of group IIA, IIIA, IVA, and IVB iron meteorites. Science 271:1099–1102

Stein H, Schersten A, Hannah J, Markey R (2003) Subgrain-scale decoupling of Re and ^{187}Os and assessment of laser ablation ICP-MS spot dating in molybdenite. Geochim Cosmochim Acta 67:3673–3686

Sun S, McDonough WF (1989) Chemical and isotopic systematics of oceanic basalts: implications for mantle composition and processes, In: Saunders AD, Norry MJ, (Eds.), Magmatism in the ocean basins: Geological Society of London Special Publication 42: 313–345

Sun WD, Huang RF, Li H, Hu YB, Zhang CC, Sun SJ, Zhang LP, Ding X, Li CY, Zartman RE, Ling MX (2015) Porphyry deposits and oxidized magmas. Ore Geol Rev 65:97–131

Sykora S, Cooke DR, Meffre S, Stephanov AS, Gardner K, Scott R, Selley D, Harris AC (2018) Evolution of pyrite trace element compositions from porphyry-style and epithermal conditions at the Lihir gold deposit: implications for ore genesis and mineral processing. Econ Geol 113:193–208

Tarkian M, Koopmann G (1995) Platinum-group minerals in the Santo Tomas II (Philex) porphyry copper-gold deposit, Luzon Island, Philippines. Mineral Deposita 30:39–47

Thiéblemont D, Stein G, Lescuyer J (1997) Gisements épithermaux et porphyriques: la connexion adakite. Comptes Rendus Academy Science Paris: Sciences de la terre et des Planetes 325:103–109

Torrence C, Compo GP (1998) A practical guide to wavelet analysis. Bull Am Meteorol Soc 79:61–78

Trail D, Watson EB, Tailby ND (2011) The oxidation state of Hadean magmas and implications for early Earth's atmosphere. Nature 480:79–82

Trotzsch U, Ellis DJ (2004) High P-T study of solid solutions in the system ZrO_2-TiO_2: the stability of strilankite. Eur J Mineral 16:577–584

Trotzsch U, Ellis DJ (2005) The ZrO_2-TiO_2 phase diagram. J Mater Sci 40:4571–4577

Tulloch AJ, Kimbrough DL (2003) Paired plutonic belts in convergent margins and the development of high Sr/Y magmatism: Peninsular Ranges batholith of Baja-California and Median batholith of New Zealand. Geological Society of America Special Paper 374:1–21

Vaughan APM (1995) Circum-Pacific mid-Cretaceous deformation and uplift: a superplume-related event? Geology 23(6):491–494

Walia M, Knitte U, Suzuki S, Chung SL, Pena RE, Yang TF (2012) No Paleozoic metamorphics in Palawan (the Philippines)? Evidence from single grain U–Pb dating of detrital zircons. J Asian Earth Sci 52:134–145

Walker BA Jr, Klemetti EW, Grunder AL, Dilles JH, Tepley FJ, Giles D (2013) Crystal reaming during the assembly, maturation, and waning of an eleven-million-year crustal magma cycle: Thermobarometry of the Aucanquilcha volcanic cluster. Contrib Mineral Petrol 165:663–682

Walther HW, Forster H, Harre W, Kreuzer H, Lenz H, Muller P, Raschka H (1981) Early cretaceous porphyry copper mineralization on Cebu Island, Philippines, dated with K–Ar and Rb–Sr methods. Geol Jahrb 48:21–35

Watson EB, Harrison TM (2005) Zircon thermometer reveals minimum melting conditions on earliest Earth. Science 308:841–844

Wolfe JA (1972) K–Ar dating in the Philippines. Journal of the Geological Society of the Philippines 26:11–12

Wolfe JA, Manuzon MS, Divis AF (1978) The Taysan porphyry copper deposit, southern Luzon Island, Philippine. Econ Geol 73:608–617

Wolfe RC, Cooke DR (2011) Geology of the Didipio region and genesis of the Dinkidi alkalic porphyry Cu-Au deposit and related pegmatites, northern Luzon, Philippines. Econ Geol 106:1279–1315

Woodhead JD, Hergt JM, Davidson JP, Eggins SM (2001) Hafnium isotope evidence for 'conservative' element mobility during subduction zone processes. Earth Planet Sci Lett 192:331–346

Yumul GP (2003) The Cretaceous southeast Bohol ophiolite complex, Central Philippines: a highly disaggregated supra-subduction zone ophiolite. J Asian Earth Sci 21:957–965

Yumul GP (2007) Westward younging disposition of Philippine ophiolites and its implication for arc evolution. Island Arc 16:306–317

Yumul GP, Balce GR, Dimalanta CB, Datuin RT (1997) Distribution, geochemistry and mineralization potentials of Philippine ophiolite and ophiolitic sequences. Ofioliti 22:47–56

Yumul GP, Dimalanta CB, Tamayo RA, Barretto JAL (2000) Contrasting morphological trends of islands in Central Philippines: speculation on their origin. Island Arc 9:627–637

Yumul GP, Dimalanta CB, Maglambayan VB, Tamayo RA (2003) Mineralization controls in island arc settings: insights from Philippine metallic deposits. Gondwana Res 6:767–776

Yumul GP, Dimalanta CB, Maglambayan VB, Marquez EJ (2008) Tectonic setting of a composite terrane: a review of the Philippine island arc system. Geosci J 12:7–17

Zhang CC, Sun WD, Wang JT, Zhang LP, Sun SJ, Wu K (2017) Oxygen fugacity and porphyry mineralization: a zircon perspective of Dexing porphyry Cu deposit, China. Geochim Cosmochim Acta 206:343–363

Zhao ZH (2010) Trace element geochemistry of accessory minerals and its applications in petrogenesis and metallogenesis. Earth Science Frontiers 17:267–286 in Chinese with English abstract

Zhou D, Sun Z, Chen H-z, Xu H-h, Wang W-y, Pang X, Cai D-s, Hu D-k (2008) Mesozoic paleogeography and tectonic evolution of South China Sea and adjacent areas in the context of Tethyan and Paleo-Pacific interconnections. Island Arc 17(2):186–207